Neuron

Article

An Activity-Mediated Transition in Transcription in Early Postnatal Neurons

Highlights

- Changes in gene-regulatory elements (GREs) mediate early postnatal neuronal maturation
- DNA methylation contributes to postnatal repression of GREs
- Activity-dependent transcription factors mediate postnatal activation of GREs

Authors

Hume Stroud, Marty G. Yang, Yael N. Tsitohay, ..., Sinisa Hrvatin, Emi Ling, Michael E. Greenberg

Correspondence

michael_greenberg@hms.harvard.edu

In Brief

The molecular mechanisms controlling brain development during early life are poorly understood. Stroud et al. characterize a postnatal switch in the transcriptional regulatory circuits that operate in maturing neurons and identify mechanisms by which neuronal activity and DNA methylation mediate this process.

Stroud et al., 2020, Neuron *107*, 1–17
September 9, 2020
https://doi.org/10.1016/j.neuron.2020.06.008

CellPress

Please cite this article in press as: Stroud et al., An Activity-Mediated Transition in Transcription in Early Postnatal Neurons, Neuron (2020), https://doi.org/10.1016/j.neuron.2020.06.008

Neuron

CellPress

Article

An Activity-Mediated Transition in Transcription in Early Postnatal Neurons

Hume Stroud,[1] Marty G. Yang,[1,2] Yael N. Tsitohay,[1] Christopher P. Davis,[1] Maxwell A. Sherman,[3,4] Sinisa Hrvatin,[1] Emi Ling,[1] and Michael E. Greenberg[1,5,*]

[1]Department of Neurobiology, Harvard Medical School, Boston, MA 02115, USA
[2]Program in Neuroscience, Harvard Medical School, Boston, MA 02115, USA
[3]Computer Science and Artificial Intelligence Laboratory, Massachusetts Institute of Technology, Cambridge, MA 02139, USA
[4]Division of Genetics, Department of Medicine, Brigham and Women's Hospital and Harvard Medical School, Boston, MA 02115, USA
[5]Lead Contact
*Correspondence: michael_greenberg@hms.harvard.edu
https://doi.org/10.1016/j.neuron.2020.06.008

SUMMARY

The maturation of the mammalian brain occurs after birth, and this stage of neuronal development is frequently impaired in neurological disorders, such as autism and schizophrenia. However, the mechanisms that regulate postnatal brain maturation are poorly defined. By purifying neuronal subpopulations across brain development in mice, we identify a postnatal switch in the transcriptional regulatory circuits that operates in the maturing mammalian brain. We show that this developmental transition includes the formation of hundreds of cell-type-specific neuronal enhancers that appear to be modulated by neuronal activity. Once selected, these enhancers are active throughout adulthood, suggesting that their formation in early life shapes neuronal identity and regulates mature brain function.

INTRODUCTION

During postnatal brain development, postmitotic neurons migrate to specific regions of the brain, form and refine their synapses, and begin to express specific neurotransmitters and neuropeptides. This maturation of neurons and neural circuits occurs in the first few years of life in humans at the time that neurological disorders, such as autism and intellectual disability, are first detected (Marín, 2016). By the time this critical period of postnatal brain development ends in late adolescence, the time when psychiatric disorders, such as schizophrenia and bipolar illness, manifest, a diverse population of neurons has been created, in which each specialized neuronal subtype has a unique function.

Gene expression patterns in large part determine neuronal identity and contribute to the differences in the properties of mature neuronal subtypes that make up the brain. Previous studies have correlated the expression of subsets of genes with the process of neuronal maturation. For example, interneuron maturation is associated with an increase in the expression of genes that encode GABA transporters (Conti et al., 2004) and $GABA_A$ receptors (Le Magueresse and Monyer, 2013), which modulate increases in firing frequency during development. At a similar postnatal time period, there is a change in NMDA glutamate receptor subunit composition (Sheng et al., 1994; Williams et al., 1993), leading to shorter NMDA-mediated excitatory postsynaptic currents (Flint et al., 1997).

A feature of postnatal brain development is its dependence upon sensory experience (Wiesel and Hubel, 1963). A variety of neuronal-activity-dependent processes have been described that are critical for brain maturation, including changes in the expression of neurotransmitters and neurotransmitter receptors and the local translation of mRNAs at synapses (Fiumelli et al., 2005; Spitzer, 2017; Yap and Greenberg, 2018). Although sensory experience is known to activate extensive programs of gene transcription within the nucleus (Chen et al., 2017; Yap and Greenberg, 2018), it is not clear whether these programs are important for postnatal neuronal maturation or exclusively regulate brain homeostasis and plasticity in the mature nervous system. An alternative possibility is that sensory-experience-independent gene expression programs couple with activity-dependent changes that occur locally at synapses to promote postnatal neuronal maturation (Berry and Nedivi, 2016).

To understand how neurons mature in normal brains and how this process goes awry in disease, we sought to identify the regulatory mechanisms that control neuronal subtype-specific gene expression in the postnatal period. Neuronal gene expression is controlled by two types of regulatory sequences: promoter sequences that function proximal to the transcriptional start site (TSS) and enhancers that function at sites that can be a long distance away from the TSS.

During brain development, it is not known when and how enhancer selection takes place. In particular, it is not clear whether the cells' enhancer repertoire is selected prior to or after the last cell division and whether or not new enhancer landscapes are selected as neurons mature in the postnatal period. Although it is known that changes in expression of specific genes

Please cite this article in press as: Stroud et al., An Activity-Mediated Transition in Transcription in Early Postnatal Neurons, Neuron (2020), https://doi.org/10.1016/j.neuron.2020.06.008

and their cognate regulatory elements (GREs) take place during postnatal brain maturation (Frank et al., 2015; Nord et al., 2013; Reilly et al., 2015; Visel et al., 2013), the molecular mechanisms that mediate these developmental changes are poorly understood.

RESULTS

Transitions in Transcription Profiles in Defined Neuronal Subtypes during Early Life

To gain insight into the developmental programs underlying neuronal maturation in the postnatal brain, we purified and compared two non-overlapping interneuron subpopulations—vasoactive intestinal peptide-expressing (*Vip*) and somatostatin-expressing (*Sst*) neurons that play distinct roles in regulating cortical circuits: *Sst* neurons are wired into neuronal networks to inhibit pyramidal neurons, whereas *Vip* neurons specialize in inhibiting *Sst* neurons, thus providing a brake on inhibition within neural circuits (Pfeffer et al., 2013; Urban-Ciecko and Barth, 2016).

To examine gene expression profiles in lineage-committed *Vip* and *Sst* neurons, we used the INTACT protocol (Mo et al., 2015) to affinity purify mouse cortical nuclei from specific neuronal subtypes at postnatal 1, 3, and 8 weeks (adults) and performed RNA sequencing (RNA-seq) (Figure 1A). These time points were chosen because most interneurons have reached the cortex by 1 week and most cortical neurons have functionally matured by 3 weeks (Le Magueresse and Monyer, 2013; Miyoshi and Fishell, 2011).

We found that *Sst*- and *Vip*-expressing neurons are present within the cortex and enriched for *Sst* and *Vip* mRNA transcripts, respectively, at 1 week of age, indicating that these neuronal subtypes are already formed at this time (Figure 1B). The 8-week (adult) *Sst* and *Vip* neuronal nuclear RNA-seq data were in general agreement with published ribosome-bound RNA-seq data from corresponding adult cell types (Mardinly et al., 2016; *Sst*: $\rho = 0.80$; *Vip*: $\rho = 0.77$; Figure S1A). Comparison of the gene expression profiles of 1-week *Sst* and *Vip* neurons suggested that, at this time, there are already substantial differences between the two subtypes (Figure S1B).

Previous work has identified several genes, including cadherin genes *Cdh7* and *Cdh11*, that distinguish subpopulations of mature *Sst* and *Vip* neurons (Paul et al., 2017). We found that these genes are already expressed in the mouse brain at 1 week of age, and their expression does not change substantially during the first 8 weeks of life, suggesting that the identity of these neurons is partly established by 1 week after birth for both *Sst* and *Vip* neuronal subtypes (Figure S1C).

It is known that, between 1 week and 3 weeks, interneurons acquire distinct morphological and electrophysiological properties (Le Magueresse and Monyer, 2013), suggesting that there could be changes in the expression of some neuronal subtype-specific genes during this time period. We found that the expression of embryonic genes is significantly downregulated between postnatal week 1 and 3, whereas other genes, including those that encode proteins with synaptic functions, became activated during this same time period (Figures 1C–1F and S1D–S1F). By contrast, fewer changes were observed between 3 weeks and 8 weeks, suggesting that changes in gene expression that occur during early postnatal life are relatively stable and persist into adulthood. These findings were confirmed by fluorescence-activated cell sorting (FACS) of *Sst*- and *Vip*-expressing nuclei followed by single-nucleus RNA-seq of immature (postnatal day 7 [P7]) or mature (8-week) neurons (Figures 1G, 1H, S1G, and S1H).

Approximately 20%–30% of the neuronal genes that are upregulated during the postnatal period are induced in a neuronal subtype-specific manner (Figure S1F). For example, *Vip* neurons, but not *Sst* neurons, express nicotinic acetylcholine receptors, *Chrna5* and *Chrna7* (Figure 1F). A feature of *Vip* neurons, but not other neuronal subtypes, is that the neurons respond to forebrain stimulation by nicotinic acetylcholine (Alitto and Dan, 2013). This suggests that postnatal activation of *Chrna5* and *Chrna7* genes confers this specific property to *Vip* neurons.

Identification of Enhancers Associated with Changes in Transcription Programs

We next characterized the molecular mechanisms that control these early life shifts in gene expression. We first identified the active promoters and enhancers across the genomes of *Sst* and *Vip* neurons at various times during the postnatal period (1 week, 3 weeks, and 8 weeks) using chromatin immunoprecipitation followed by sequencing (ChIP-seq) for histone H3 lysine 27 acetylation (H3K27ac), a histone mark that is present at active promoters and enhancers (Heintzman et al., 2009).

We performed ChIP-seq using anti-H3K27ac antibodies to generate genome-wide maps of all putative active GREs in *Sst* and *Vip* neurons within mouse cortices at each postnatal stage. We identified over 30,000 putative active GREs for each neuronal subtype at each postnatal stage (Figures 2A, 2B, S2A, and S2B). We performed ATAC-seq on *Sst* and *Vip* neurons at 1 week and 8 weeks. ATAC-seq is a method that assesses chromatin accessibility based on *in vitro* transposase accessibility to chromatin (Buenrostro et al., 2013) and allows GREs, such as enhancers, promoters, and insulators, to be mapped at higher resolution than that achieved using histone modifications alone (see STAR Methods).

To identify postnatally regulated enhancers, we defined ATAC-seq peaks where flanking H3K27ac levels (±500 bp from ATAC-seq peak summits) significantly change between immature and mature neurons (>2-fold; false discovery rate [FDR] < 0.01 cutoff). These analyses resulted in identification of hundreds of genomic sites where the level of H3K27ac changes significantly during postnatal neuronal development (Figures 2C and S2C). Essentially all changes in the H3K27ac level were detected between 1 and 3 weeks, coinciding with the timing of changes in gene expression described above (Figure 1). Importantly, by analyzing aged mice (~20 months), we confirmed that postnatally repressed or activated enhancers are maintained in the repressed or activated state, respectively, throughout adulthood (Figure 2C). Although changes in H3K27ac were also detected at the promoters of genes whose expression changes during the postnatal period, we observed that about 90% of the significant changes in H3K27ac occurred at least 1 kb away from all annotated transcription start sites (Figure 2D). We defined H3K27ac regions that are at least 1 kb distal to an

Please cite this article in press as: Stroud et al., An Activity-Mediated Transition in Transcription in Early Postnatal Neurons, Neuron (2020), https://doi.org/10.1016/j.neuron.2020.06.008

CellPress

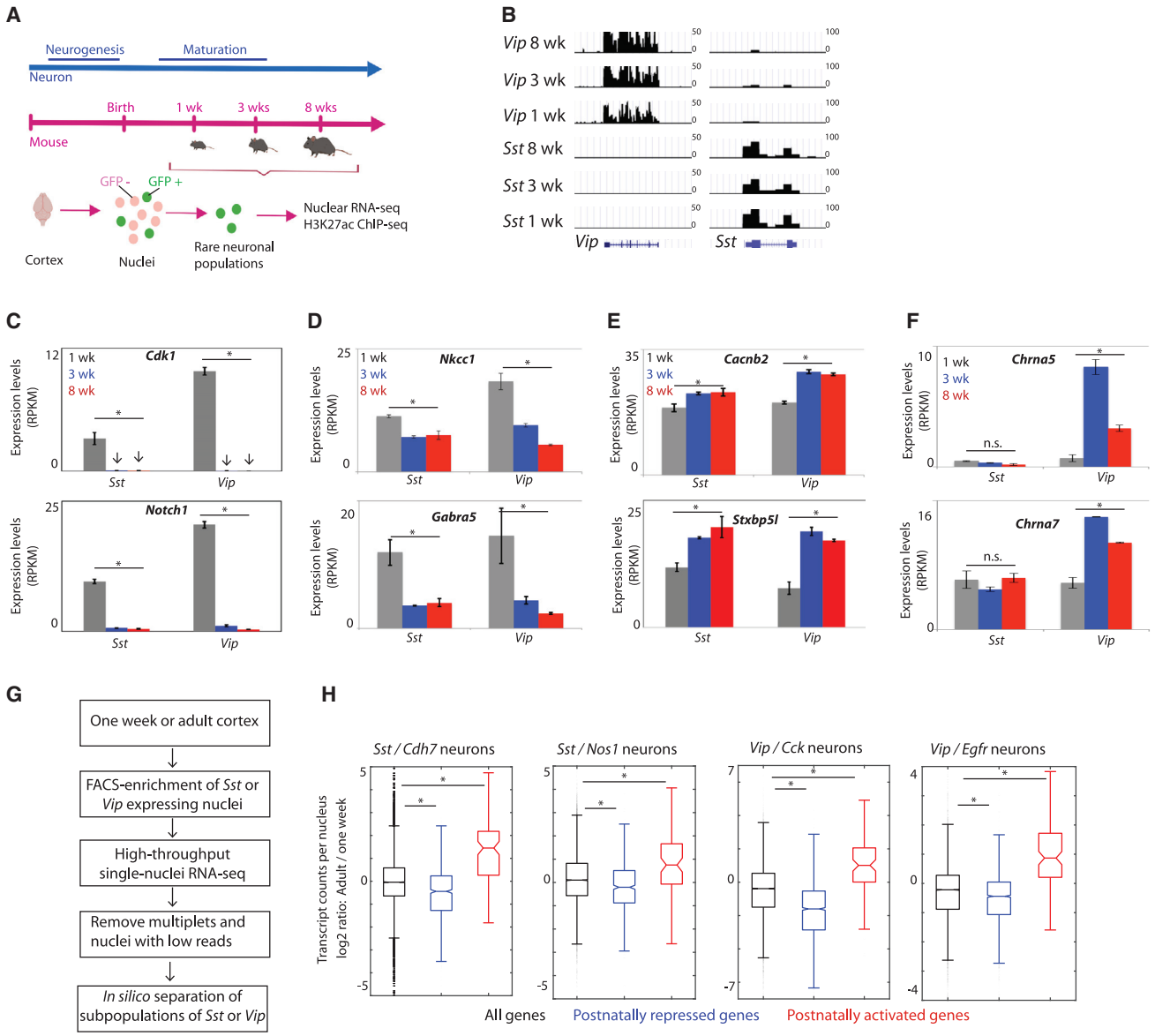

Figure 1. Dynamic Changes in Neuronal Gene Expression Programs within Early Postnatal Brains

(A) An overview of the experimental design.

(B) Genome browser views confirming specific enrichment of *Sst* and *Vip* transcripts in INTACT-isolated *Sst*- and *Vip*-expressing nuclei, respectively. The y axis units represent reads per kilobase per million mapped reads (RPKM). At the bottom of the panel, the exon and intron structure of the *Sst* and *Vip* genes is shown.

(C) Normalized expression levels of representative genes that are postnatally repressed encoding proteins involved in embryogenesis. Error bars represent SD between biological replicates. *FDR < 1e–4; DEseq2.

(D) Normalized expression levels of representative genes that are postnatally repressed encoding co-transporters and receptors. *FDR < 1e–4; DEseq2.

(E) Normalized expression levels of representative genes that are postnatally activated encoding proteins involved in synaptic function. *FDR < 1e–4; DEseq2.

(F) Normalized expression levels of representative genes that are selectively postnatally activated in *Vip* neurons, but not in *Sst* neurons. *FDR < 1e–4; DEseq2.

(G) Scheme of the experimental design for high-throughput single-nucleus RNA sequencing of FACS-sorted *Sst*- or *Vip*-expressing nuclei.

(H) Postnatal regulation of gene expression in neurons is a shared feature across subpopulations of *Sst* and *Vip* neurons. The normalized mean transcript counts per nucleus in different subpopulations of *Sst* or *Vip* neurons were calculated across all genes (black bars), postnatally repressed genes (defined by INTACT RNA-seq, blue bars), and postnatally activated genes (defined by INTACT RNA-seq, red bars). *Sst* subpopulations expressing *Cdh7* or *Nos1* and *Vip* subpopulations expressing *Cck* or *Egfr* are shown. Genes that were not expressed at either developmental time points were excluded from the analysis. *p < 1e–5; Wilcoxon rank sum test.

Please cite this article in press as: Stroud et al., An Activity-Mediated Transition in Transcription in Early Postnatal Neurons, Neuron (2020), https://doi.org/10.1016/j.neuron.2020.06.008

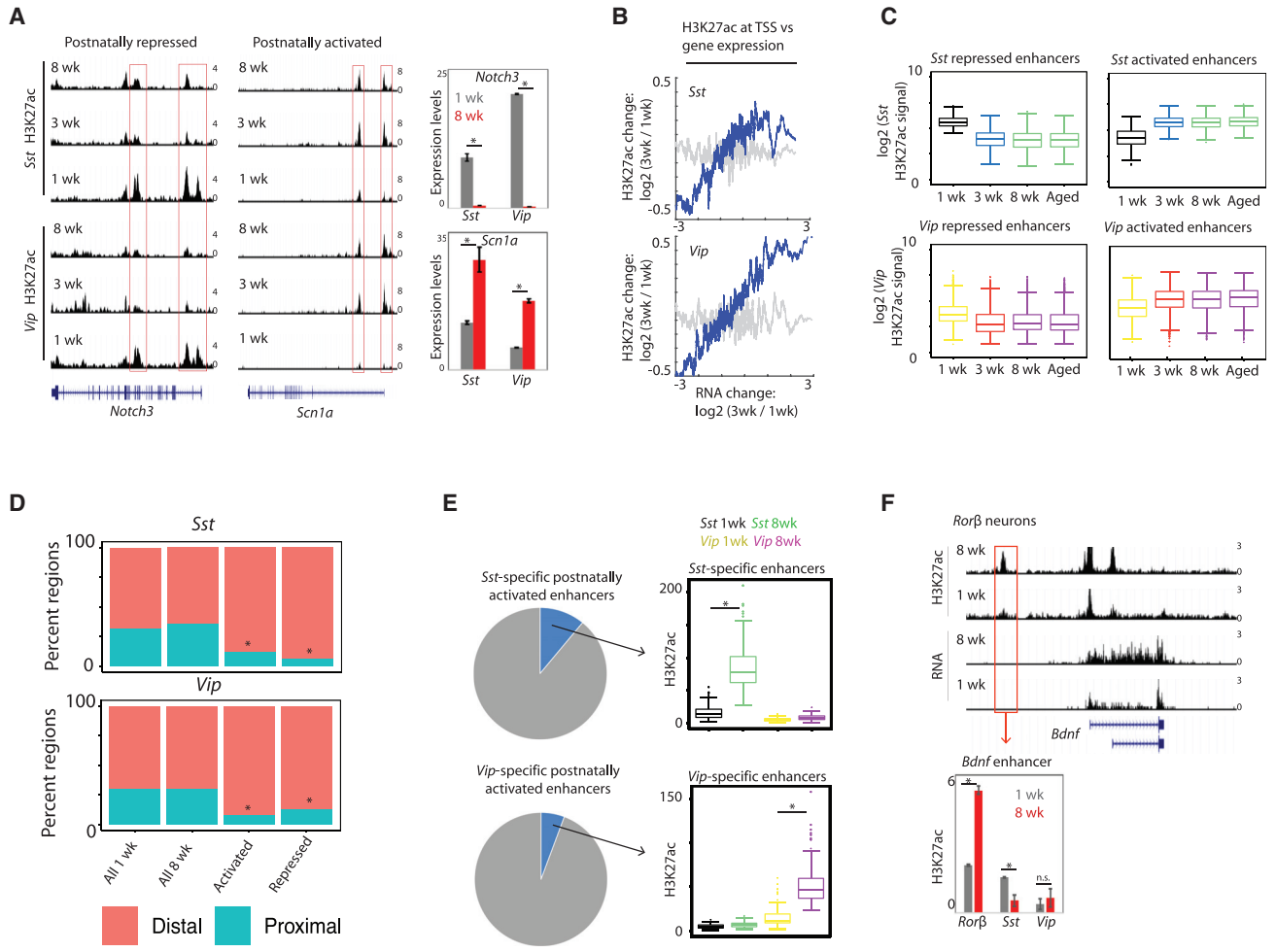

Figure 2. Dynamic Gene-Distal Enhancers Reflect Early Postnatal Changes in Transcription Profiles

(A) Genome browser views of H3K27ac patterns in *Sst* and *Vip* neurons. H3K27ac patterns across a postnatally repressed gene (*Notch3*; left) and an activated gene (*Scn1a*; right) are shown. The gene expression levels of the two genes are also shown. Error bars represent SD between biological replicates. *FDR < 1e–4; DEseq2.

(B) Genome-wide correlation between postnatal changes in gene expression and postnatal changes in H3K27ac at TSS. The average postnatal changes (between 1 week and 3 weeks) in H3K27ac read densities within 500 bp of annotated TSS were binned according to the postnatal changes in gene expression levels (200 genes per bin). H3K27ac levels after random grouping of genes are shown as controls in faded gray lines. $p < 0.001$; permutation test.

(C) Most postnatal changes in H3K27ac occur by 3 weeks after birth in both *Sst* and *Vip* neurons. Genomic regions that significantly change in H3K27ac levels between 1 week and adult (8 weeks) were defined (±500 bp of ATAC-seq summit; see STAR Methods), and densities of H3K27ac at 1 week, 3 weeks, 8 weeks, and aged (~20 months) were plotted.

(D) Most postnatal changes in H3K27ac occur at gene-distal sites. Proportion of H3K27ac regions proximal to promoters or distal to genes (i.e., greater than 1 kb away from nearest annotated TSS) are shown. *p < 1e–4; hypergeometric distribution.

(E) A subset of enhancers is selectively activated postnatally in either *Sst* (n = 91) or *Vip* (n = 116). Enhancers that were significantly activated in *Sst*, but not *Vip*, and vice versa were defined. *p < 1e–7; Wilcoxon rank sum test.

(F) A postnatally activated enhancer in *Rorβ* neurons upstream of the *Bdnf* gene. Genome-browser views of gene expression and H3K27ac signal, as well as quantifications of H3K27ac within the distal *Bdnf* enhancer in *Rorβ*, *Sst*, and *Vip* neurons are shown. *p < 0.05; two-tailed t test.

annotated TSS as putative active enhancers. These findings indicate that most changes in GRE activity during postnatal neuronal development occur at enhancers that are distal to genes, suggesting that these genomic elements control the postnatal transcriptional changes.

We next linked the gene-distal changes in H3K27ac regions to the closest TSS of genes and found that decreases in H3K27ac were significantly associated with genes whose transcription is downregulated during the postnatal period, whereas the increases in H3K27ac were associated with genes whose transcription is upregulated during this time period (Figure S2D). Thus, the postnatal developmental shifts in the activity of gene-distal enhancers are tightly correlated with postnatal gene expression changes.

Because the transcriptional activation of genes during postnatal neuronal development is in part neuronal subtype-specific,

Please cite this article in press as: Stroud et al., An Activity-Mediated Transition in Transcription in Early Postnatal Neurons, Neuron (2020), https://doi.org/10.1016/j.neuron.2020.06.008

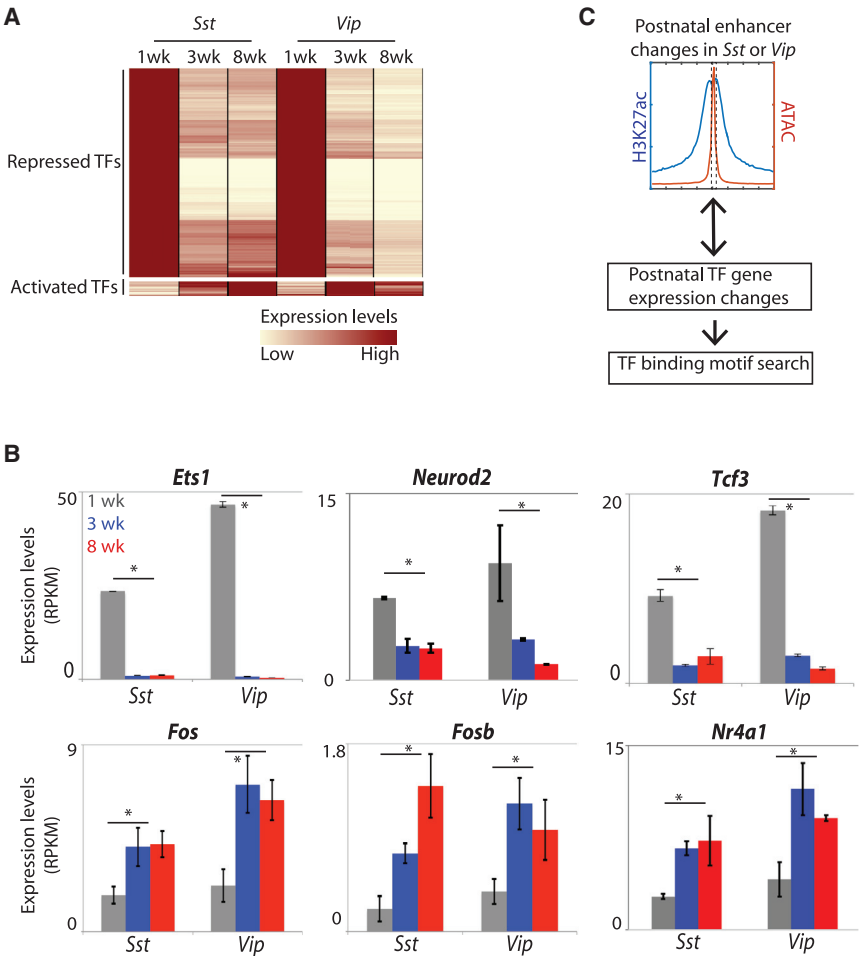

Figure 3. Putative Regulatory TFs Control the Postnatal Switch in Transcription Programs

(A) Identification of TFs that change in gene expression during maturation. Gene expression heatmaps of TFs that postnatally decrease in expression in either *Sst* or *Vip* (top; n = 200) or increase in expression in either *Sst* or *Vip* neurons (bottom; n = 15) during maturation are shown (>2-fold; FDR < 1e–4 cutoff). The expression level of a given gene was normalized to the highest value across the indicated time course.

(B) Representative examples of TFs that are postnatally repressed or activated. *FDR < 1e–4; DE-seq2. Error bars represent SD between biological replicates.

(C) Approach for identifying regulatory TFs controlling postnatally repressed or activated enhancers.

we examined whether changes in H3K27ac also occur in a subtype-specific manner. This analysis revealed that a subset of enhancers is activated in a subtype-specific manner during the postnatal period (Figures 2E and S2E). To control for genetic differences between the two mouse strains that could in principle lead to differential enhancer activity, we analyzed unpurified nuclei (i.e., not selected for *Sst*- or *Vip*-expressing nuclei) from each mouse strain and confirmed that there are no significant differences in enhancer activity between the two mouse strains. This suggests that the neuronal subtype-specific postnatal enhancer activation is not driven by genetic differences between the two strains of mice (Figure S2F).

We next asked whether these enhancers have human orthologs that are enriched for genetic variants associated with disease. Using a partitioned heritability approach by linkage disequilibrium-score regression (Finucane et al., 2015), we find that both *Sst* and *Vip* postnatally activated enhancers, as well as constitutively active postnatal enhancers that are conserved between mice and humans, are significantly enriched for genetic variants associated in schizophrenia (Figure S2G). In contrast, there is no statistically significant enrichment for these genetic variants within the set of enhancers that are repressed as the brain matures postnatally. In addition, there is no enrichment within the *Sst* or *Vip* postnatally activated enhancer sets for genetic variants that are associated with other neurological disorders, such as Alzheimer's disease and amyotrophic lateral sclerosis, or with other human disorders, including eczema and cardiac diseases.

We assessed whether the reorganization of enhancers that we detect in *Sst* and *Vip* interneurons early after birth is specifically a feature of interneurons. To this end, we examined the postnatal developmental dynamics of enhancers and gene transcription in *Rorβ*-expressing nuclei. *Rorβ* is expressed selectively in excitatory neurons that form layer IV of the cortex, a brain region that initiates sensory processing in the cortex (Molyneaux et al., 2007). We isolated *Rorβ*-expressing nuclei from P7 and 8-week cortices and confirmed that *Rorβ* neurons also undergo postnatal changes in enhancer landscapes and gene expression programs (Figures 2F and S2H–S2J). Enhancers that are postnatally activated in *Rorβ* neurons were largely distinct from those observed in *Sst* or *Vip* neurons (Figure S2K).

Identification of Putative TFs that Orchestrate Postnatal Changes in Neuronal Enhancer Profiles

To identify mechanisms by which cohorts of enhancers are decommissioned or licensed during postnatal neuronal maturation, we searched our RNA-seq data from each neuronal subtype for transcription factors (TFs) that are differentially expressed in immature neurons compared to mature neurons and thus might regulate the neuronal maturation gene expression switch. We identified a large number of TFs (N = 200) that are downregulated upon maturation, whereas a more limited number of TFs (N = 15) are upregulated (Figure 3A). The TFs significantly downregulated as neurons mature are largely overlapping between *Sst* and *Vip* neurons (>90% overlap), suggesting a shared regulatory mechanism by which neurons turn down gene expression. We identified genes encoding chromatin remodelers and transcriptional

Please cite this article in press as: Stroud et al., An Activity-Mediated Transition in Transcription in Early Postnatal Neurons, Neuron (2020), https://doi.org/10.1016/j.neuron.2020.06.008

activators that are highly expressed in immature neurons but are downregulated as neurons mature, including members of the *Ets*, *Neurod*, *Tcf*, and *Sox* families that are known to play a role in early neuronal differentiation and cell fate determination (Figures 3B and S3A). By aligning the ATAC-seq data with the H3K27ac maps and searching for an enrichment of TF motifs within these regulatory sequences (Figure 3C), we found that the binding sites for TCF3 and NEUROD TFs are enriched within the enhancers that are downregulated during postnatal neuronal development, raising the possibility that these enhancers might in part be activated by TCF3, NEUROD, and other TFs in immature neurons and that the subsequent downregulation of TCF3 and NEUROD expression might contribute to the repression of these enhancers as neurons mature after birth (Figure S3B).

De Novo DNA Methylation Promotes Transcriptional Repression by Decommissioning Embryonic GREs

We asked whether additional mechanisms might also contribute to the inactivation of enhancers during the postnatal period, such as the methylation of cytosines and recruitment of methylcytosine binding repressor proteins. DNA methylation is essential for normal brain development, inasmuch as mutations in DNMT3A, the enzyme that catalyzes cytosine methylation in the brain, have been found to be a cause of autism spectrum disorder (ASD) and/or intellectual disabilities (Sanders et al., 2015; Tatton-Brown et al., 2014). In neurons, DNA methylation accumulates during the first few weeks of life (Lister et al., 2013), coinciding with the timing of postnatal neuronal enhancer repression. Notably, embryonic enhancers that become repressed in adult cortices acquire DNA methylation, suggesting a role for DNA methylation in enhancer repression (Lister et al., 2013; Mo et al., 2015). To investigate this possibility further using defined subsets of postmitotic neurons, we performed whole-genome bisulfite sequencing (WGBS) on *Sst* neurons at the 1-, 3-, and 8-week time points to generate base-resolution maps of DNA methylation in developing *Sst* neurons (Figures 4A and S4A). We then compared these datasets with each other and with WGBS data obtained from similarly prepared *Vip* neurons (Stroud et al., 2017). Differential methylation analyses identified discrete regions (mean size ~200 bp) that significantly increase in methylation in *Sst* and *Vip* neurons between 1 and 3 weeks after birth. About 90% of these increased methylated regions (IMRs) are located at gene-distal sites, and gene-ontology analyses significantly associated the IMRs with genes involved in embryonic development (Figure S4B), suggesting that the majority of the IMRs may be embryonic GREs (eGREs). To assess the role of the postnatal increase in DNA methylation on postnatal enhancer repression, we focused on IMRs that are still open (ATAC signal is detected) at 1 week after birth but become inactivated by 8 weeks (ATAC signal is not detected; Figure S4C).

To determine whether cytosine methylation contributes to eGRE repression, we assessed the effect of blocking enhancer cytosine methylation by disrupting the function of DNMT3A. We first asked whether DNMT3A is required for methylation at the regulatory elements using *Sst*-cre or *Vip*-cre mice crossed to *Dnmt3a*$^{fl/fl}$ and SUN1 mice to specifically delete DNMT3A in *Sst* or *Vip* neurons (*Sst*-cre; *Dnmt3a*$^{fl/fl}$; *Sun1* and *Vip*-cre; *Dnmt3a*$^{fl/fl}$; *Sun1*). *Sst*- or *Vip*-expressing nuclei were INTACT purified from the adult cortex from knockout (KO) or wild-type littermate controls (*Sst*-cre; *Dnmt3a*$^{+/+}$; *Sun1* and *Vip*-cre; *Dnmt3a*$^{+/+}$; *Sun1*; Figure 4B). We generated base-resolution maps of DNA methylation from INTACT-purified *Sst*- or *Vip*-expressing nuclei (Figure S4D) and focused our analysis on methylation at the eGRE sequences. We found that, in *Dnmt3a* KO neurons compared to wild-type neurons, there is a significant decrease in cytosine methylation at eGREs (Figure 4C), confirming that DNMT3A mediates the postnatal increase in methylation at these sequences.

We next performed H3K27ac and H3K4me1 ChIP-seq analyses on adult (>8-weeks-old) *Sst*- or *Vip*-specific *Dnmt3a* conditional KO neurons. When compared to wild-type neurons, in the *Dnmt3a* conditional KO neurons, eGREs as an aggregate display a modest but reproducible increase in both H3K27ac and H3K4me1 (Figures 4D and S4E), suggesting that, in wild-type neurons, DNA methylation in part contributes to the inactivation of eGREs.

Finally, we sought to gain mechanistic insights into how DNMT3A-mediated methylation represses eGREs. One way by which methylation exerts its effect is via the recruitment of methylation-reader proteins to the DNA. The methyl-DNA binding protein, MECP2, binds to methylated cytosines across the neuronal genome and recruits the transcription co-repressor NCOR (Lyst et al., 2013; Skene et al., 2010). Mutations in MECP2 give rise to Rett syndrome, a postnatal development disorder that is a common cause of severe neurologic impairment in females (Chahrour and Zoghbi, 2007). Although MECP2 has recently been shown to regulate enhancers (Clemens et al., 2020), whether MECP2 plays a role in repression of eGRE activity is not known. We hypothesized that MECP2 binds to the methylated cytosines across the eGREs (Figure S4F) and recruits the transcription co-repressor NCOR to exert eGRE repression. To investigate this possibility, we analyzed MECP2 binding patterns in adult DNMT3A KOs (*Nestin-cre; Dnmt3a*$^{fl/fl}$; *Dnmt3a* cKO) and *Mecp2* KO cortices and in their respective littermate wild-type control cortices. We performed CUT&RUN, a sensitive assay that allows for *in situ* mapping of protein-DNA interactions in native chromatin states across the genome (Skene and Henikoff, 2017). We detect MECP2 binding across eGREs in adult wild-type, but not in adult *Mecp2* KO, cortex, thus confirming the specificity of the anti-MECP2 antibody for detecting MECP2 binding to DNA (Figure 4E). Upon deletion of DNMT3A, MECP2 binding across eGREs is significantly reduced, suggesting that MECP2 is recruited to these sites by DNMT3A-mediated methylation (Figure 4F). Similar to our observations using conditional *Sst*- and *Vip*-specific *Dnmt3a* KO neurons, we observed increases in H3K27ac at eGREs in whole brain-specific *Dnmt3a* cKO cortices compared to wild-type cortices, suggesting that, upon DNMT3A deletion, these sites become more active (Figures 4G and S4G). Deletion of MECP2 results in only a modest increase in H3K27ac at eGREs compared to the effect seen in the *Dnmt3a* cKO cortices, suggesting that, although MECP2 contributes to eGRE repression, it is not the only factor that mediates repression of these sites (Figures 4G and S4G). These findings

Please cite this article in press as: Stroud et al., An Activity-Mediated Transition in Transcription in Early Postnatal Neurons, Neuron (2020), https://doi.org/10.1016/j.neuron.2020.06.008

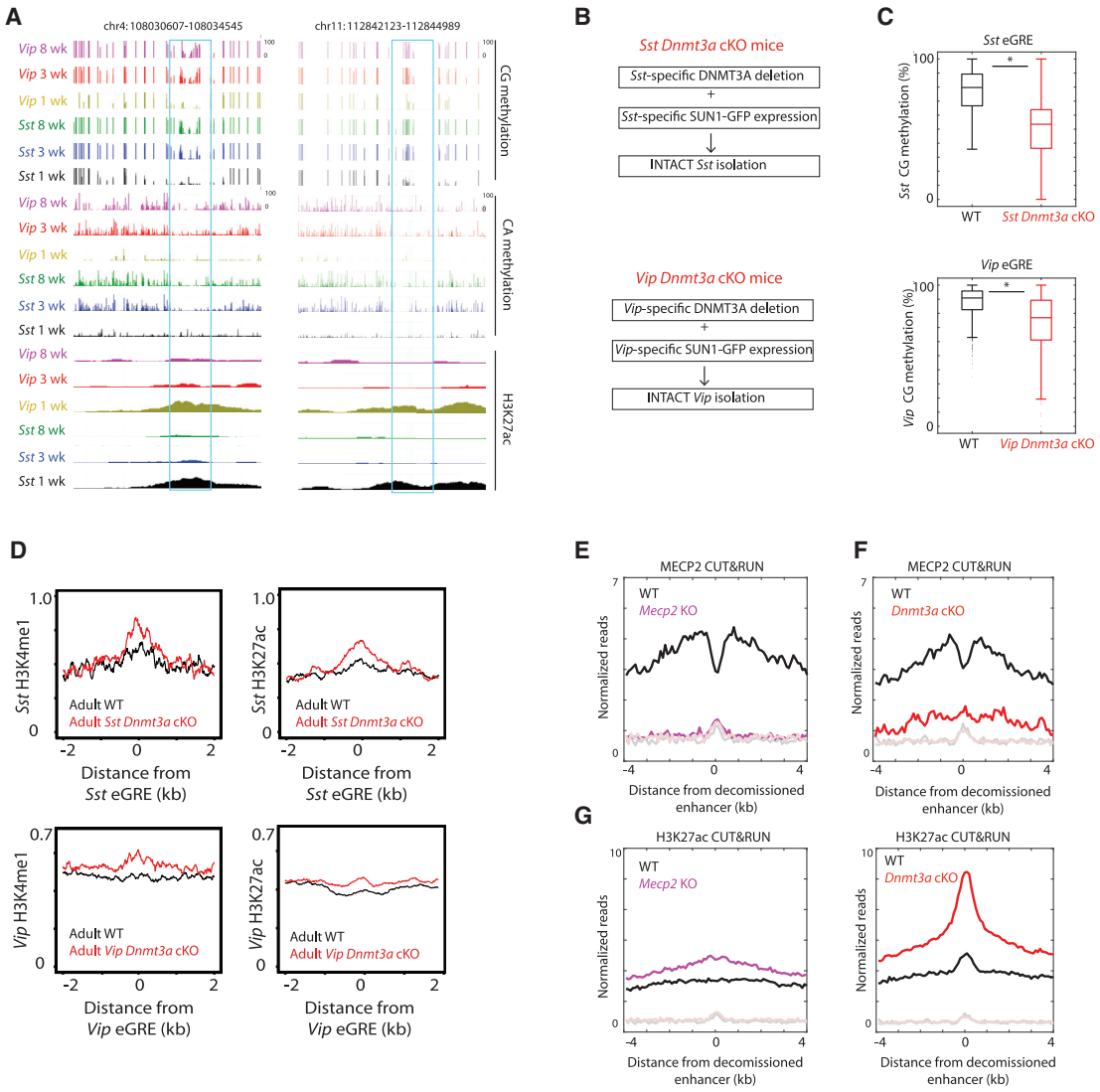

Figure 4. *De Novo* Methylation-Mediated Enhancer Decommissioning

(A) Genome-browser views of base-resolution DNA methylation data across two gene-distal postnatally repressed enhancers.

(B) Cell-type-specific DNMT3A deletion and analysis. In *Sst*-specific *Dnmt3a* cKO mice, both DNMT3A deletion and SUN1-GFP expression selectively occurs in *Sst* neurons. In *Vip*-specific *Dnmt3a* cKO mice, both DNMT3A deletion and SUN1-GFP expression selectively occurred in *Vip* neurons. This strategy enabled INTACT purification of *Sst*- or *Vip*-expressing nuclei for further analyses.

(C) DNMT3A mediates the postnatal CG methylation at embryonic GREs (eGREs). Adult CG methylation was quantified within eGREs in *Sst* and *Vip* neurons. *Dnmt3a* KO *Sst* neurons from *Sst*-specific *Dnmt3a* cKO mice were compared to wild-type *Sst* neurons from littermate wild-type mice. *Dnmt3a* KO *Vip* neurons from *Vip*-specific *Dnmt3a* cKO mice were compared to wild-type *Vip* neurons from littermate wild-type mice. *p < 1e–18; Wilcoxon rank sum test.

(D) Increase in enhancer activity of eGREs is observed in adult *Sst Dnmt3a* KO (top) or *Vip Dnmt3a* KO (bottom) neurons compared to wild type. The average distribution of H3K4me1 and H3K27ac in adult (>8 weeks) wild-type or *Dnmt3a* KO neurons across eGREs were plotted.

(E) MECP2 binding is enriched across eGREs in whole cortex. Average MECP2 CUT&RUN read distribution in adult wild-type and *Mecp2* KO cortices across eGREs that normally gain methylation postnatally (shown in Figure S4F) was plotted. Faded lines represent respective IgG controls.

(F) MECP2 binding across eGREs is reduced upon deletion of DNMT3A. Average MECP2 CUT&RUN read distribution in wild-type and *Dnmt3a* cKO cortices across eGREs. Faded lines represent respective IgG controls.

(G) Enhancer activity increases in eGREs in adult *Mecp2* or *Dnmt3a* cKO cortices. Average H3K27ac CUT&RUN read distribution across GREs in wild-type and *Mecp2* KO (left) or *Dnmt3a* cKO cortices (right) across eGREs. Faded lines represent respective IgG controls. Note that the IgG controls shown here are the same as those in (E) and (F).

suggest that cytosine methylation and MECP2 binding facilitate eGRE repression in part via MECP2 recruitment. Due to its stability, DNA methylation is an attractive mechanism for achieving long-term enhancer silencing in neurons—postmitotic cells that survive and function for the lifetime of an animal.

Please cite this article in press as: Stroud et al., An Activity-Mediated Transition in Transcription in Early Postnatal Neurons, Neuron (2020), https://doi.org/10.1016/j.neuron.2020.06.008

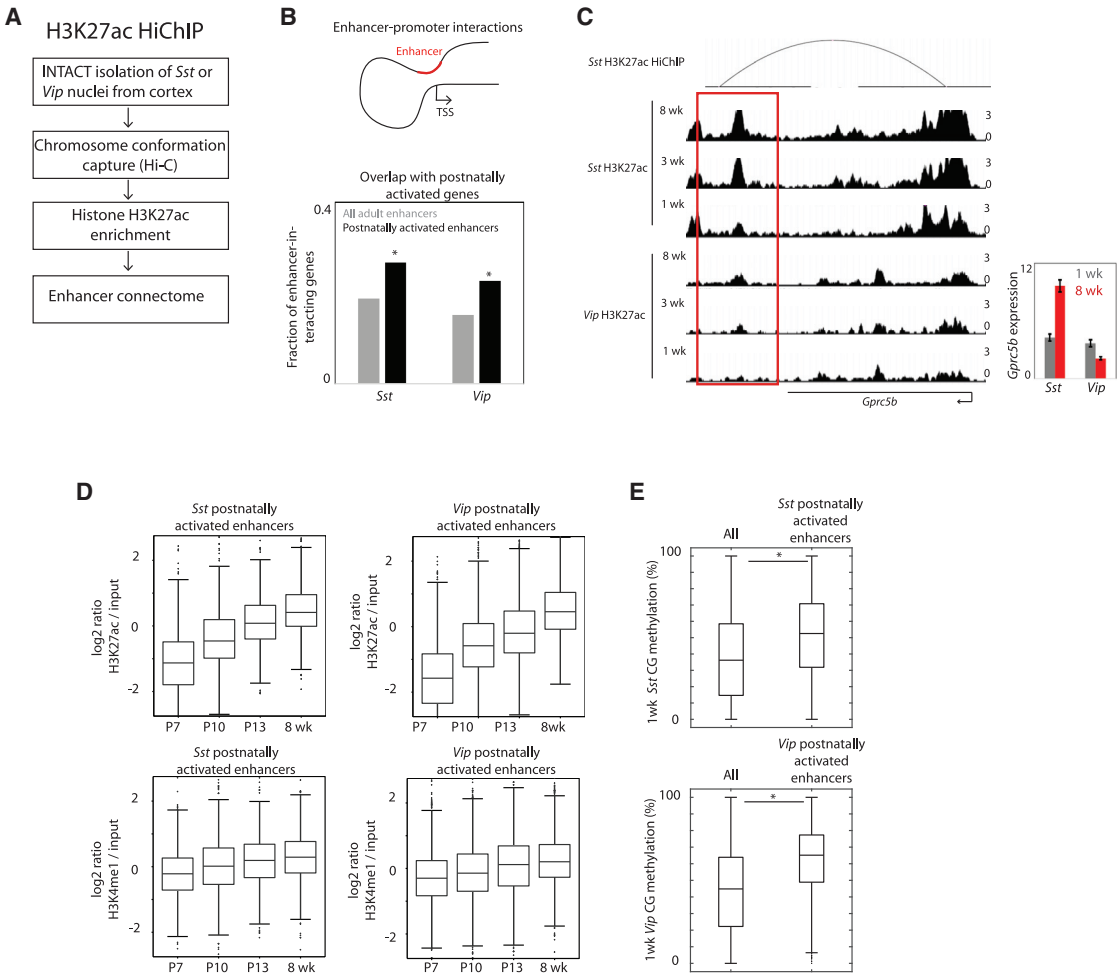

Figure 5. Formation of *De Novo* Enhancers that Promote the Postnatal Switch

(A) Workflow of using *in situ* chromatin conformation HiChIP analysis to determine enhancer connectomes in *Sst* and *Vip* neurons *in vivo*.

(B) Postnatally activated enhancers significantly interact with genes that increase in expression levels postnatally. Gene-distal enhancers (i.e., at least 1 kb away from nearest annotated TSS) were linked to genes they interact with at the TSS (i.e., TSS ± 500 bp). *p < 0.01; hypergeometric distribution.

(C) A postnatally *Sst*-specific activated enhancer downstream of the *Gprc5b* gene that physically interacts with the TSS. The gene expression levels of *Gprc5b* are also shown. Error bars represent SD between biological replicates.

(D) Co-acquisition of H3K4me1 and H3K27ac marks during the postnatal period. H3K4me1 and H3K27ac levels were quantified within postnatally activated enhancers that lack H3K27ac at P7 (i.e., are inactive at P7).

(E) Prior to activation, postnatally activated enhancers tend to be marked by CG methylation. Methylation levels at P7 were quantified across GREs within all enhancers and postnatally activated enhancers. *p < 1e–41; Wilcoxon rank sum test.

De Novo Formation of Enhancers that Shape Neuronal Identities during Early Life

A difference between the genes that are repressed during maturation and genes that increase in expression is that the postnatal increase in gene expression occurs in a manner that is partially cell type specific. Although the gene closest to the enhancer is often the target of the enhancer, recent studies have demonstrated this rule does not always hold true (Javierre et al., 2016; Mifsud et al., 2015). To understand how neuronal subtype-specific activation of enhancers and their target genes occurs, we linked the changes in gene-distal H3K27ac to their neuronal subtype-specific target genes in each neuronal subtype *in vivo* by applying the H3K27ac HiChIP protocol (Mumbach et al., 2016) to INTACT-purified *Sst*- and *Vip*-expressing nuclei isolated from the brain (Figures 5A, S5A, and S5B). This analysis revealed that postnatal enhancer activation is significantly associated with an increase in the interaction of these same enhancers with the promoters of genes that display an increase in their expression in the postnatal period (Figure 5B). In particular, we observed clear instances of genes that are newly expressed postnatally in a cell-type-specific manner that are associated with cell-type-specific enhancer activation (Figure 5C).

Conventional mechanisms of enhancer activation during embryonic development suggest that enhancers are specified prior to differentiation and that these enhancers are then kept in a state in which they are poised for activation, but not yet active.

Please cite this article in press as: Stroud et al., An Activity-Mediated Transition in Transcription in Early Postnatal Neurons, Neuron (2020), https://doi.org/10.1016/j.neuron.2020.06.008

In this state, enhancers have been shown to be marked by the histone modification H3K4me1 but lack the H3K27ac mark (Calo and Wysocka, 2013). Once differentiation occurs, the enhancer acquires H3K27ac such that active enhancers are co-marked by H3K4me1 and H3K27ac. However, other studies have found that enhancers can also form *de novo* and be immediately activated, for example, when a cell is exposed to an extracellular stimulus (Ostuni et al., 2013). To determine whether these or other mechanisms explain the activation of neuronal enhancers in the postnatal period, we performed H3K4me1 ChIP-seq at P7, P10, and P13 and examined deposition of the H3K4me1 and H3K27ac marks at these enhancers across the 7-day postnatal time course. We focused on enhancers that completely lack H3K27ac at P7 (i.e., inactive state) but significantly increase their level of H3K27ac as neurons mature. In both *Sst* and *Vip* neurons, we found that all postnatally activated neuronal enhancers lack H3K4me1 at P7 (no significant enrichment of H3K4me1 detected at any of these enhancers; Figures 5D and S5C). As neurons mature, we detected an increase in H3K4me1 with a time course that is similar to that observed for H3K27ac. This suggests that postnatally activated neuronal enhancers are not poised to be activated in early stages of development but rather are created *de novo* as neurons mature in the postnatal brain.

Because DNA methylation patterns are negatively correlated with the activation state of enhancers, we assessed the methylation status of postnatally activated neuronal enhancers. By WGBS sequencing, we observed that, prior to the activation of these enhancers, the genomic sequences that give rise to them tend to be marked by DNA methylation (Figure 5E). Moreover, we found that the formation of postnatal neuronal enhancers is associated with a decrease in cytosine methylation at these sites (Figures S5D and S5E). The decrease in cytosine methylation was largely restricted to the early postnatal period, as there were no substantial changes in DNA methylation at later times.

These results reveal that, as neurons mature in early life, new enhancers are generated. In the 1-week-old brain, these genomic elements lack histone modifications that are associated with primed enhancers and instead are marked by DNA methylation, suggesting that, at this stage, the enhancers are likely inactive and not yet poised for activation. As the neurons mature, enhancers form by co-acquiring both H3K4me1 and H3K27ac. These data argue against a model where mature neuronal function is entirely determined at the progenitor stage but instead suggests that, at least in part, neuronal function is specified early in postnatal life via *de novo* formation of enhancers.

Genome-wide Analysis Identifies AP1 TFs as Mediators of Postnatal Enhancer Activation

To identify TFs that mediate enhancer activation in postnatal neurons, we compared the expression levels of TFs between immature and mature neurons. From our RNA-seq data, we find that TFs important for establishing neuronal identity at earlier developmental stages, such as *Lhx6* and *Sox6* in *Sst* neurons and *Prox1* and *Sp8* in *Vip* neurons (Kessaris et al., 2014), continue to be expressed throughout postnatal development but are not upregulated during neuronal maturation (Figure S6A). In addition, we failed to detect any neuronal subtype-specific TFs that are upregulated as neurons mature. Instead, we found that levels of key activity-regulated TFs, such as AP1 family TFs (e.g., *Fos* and *Jun* family TFs), *Nr4a1*, and *Npas4*, increase significantly as *Sst* and *Vip* neurons mature (Figure 3). Because AP1 TFs and NPAS4 are thought to function by binding and activating specific GREs in a neuronal-activity-dependent manner, we hypothesized that, as neurons mature, stimulus-induced TFs may bind to new GREs and perhaps together with pre-existing neuronal subtype-specific TFs mediate enhancer formation.

To determine whether stimulus-dependent TFs bind to postnatally activated neuronal enhancers, we used our H3K27ac and ATAC-seq datasets obtained from *Sst* and *Vip* neurons at various times during the postnatal period (1 and 8 weeks) to identify the sequence elements within the postnatal enhancers that bind TFs and searched these elements for sequence motifs that are known to bind neuronal-activity-regulated TFs. We found that enhancers that become selectively activated in the postnatal period are enriched for the sequence TGA(C/G)TCA, the binding sites for AP1 (e.g., FOS/JUN family heterodimers), relative to all ATAC-seq peaks as well as postnatally repressed enhancers (Figure S6B).

We next asked whether AP1 TFs bind to postnatally activated neuronal enhancers in the mouse brain. Using FACS-isolated *Sst* or *Vip* nuclei from 3-week-old *Sst*-cre or *Vip*-cre; *Sun1* mouse cortices, respectively, we performed CUT&RUN with anti-FOS antibodies to examine where in the genome FOS binds across the *Sst* and *Vip* neuronal genomes (Figure 6A). As negative controls, CUT&RUN using immunoglobulin G (IgG) was performed in parallel for each biological sample. Within a FOS CUT&RUN-enriched genomic region, the DNA physically bound by FOS is protected from cleavage by micrococcal nuclease (MNase). We thus sought to perform foot-printing analyses for FOS CUT&RUN-enriched regions. Footprints within FOS CUT&RUN-enriched regions were significantly enriched for AP1 motifs, whereas similar analyses on the control IgG CUT&RUN samples did not identify significant enrichments for AP1 motifs, suggesting that FOS CUT&RUN reflects specific FOS binding events (Figures 6B and S6C). Analysis of this dataset revealed that FOS binding is enriched within postnatally activated neuronal enhancers (Figure 6C).

Because FOS TFs are lowly expressed in cells in the absence of an extracellular stimulus (Lacar et al., 2016), we hypothesized that the binding of FOS at postnatal activated enhancers likely is due to the stimulation of these neurons during their postnatal maturation. We demonstrated that FOS binding to these sites is induced by neuronal activity by exposing 3-week-old *Vip-cre; Sun1* mice to the glutamate receptor agonist kainic acid (KA), purifying the *Vip*-expressing nuclei, and using the CUT&RUN procedure to assess FOS binding across the genome (Figures S6D and S6E).

We note that our characterization of postnatal enhancers in *Sst* and *Vip* neurons that bind FOS revealed that a subset of these enhancers is specified during the postnatal period in a neuronal subtype-specific manner (Figure 2). However, in both *Sst* and *Vip* neurons, although neuronal subtype-specific TFs are present (e.g., *Lhx6* and *Sox6* in *Sst* neurons and *Prox1* and

Please cite this article in press as: Stroud et al., An Activity-Mediated Transition in Transcription in Early Postnatal Neurons, Neuron (2020), https://doi.org/10.1016/j.neuron.2020.06.008

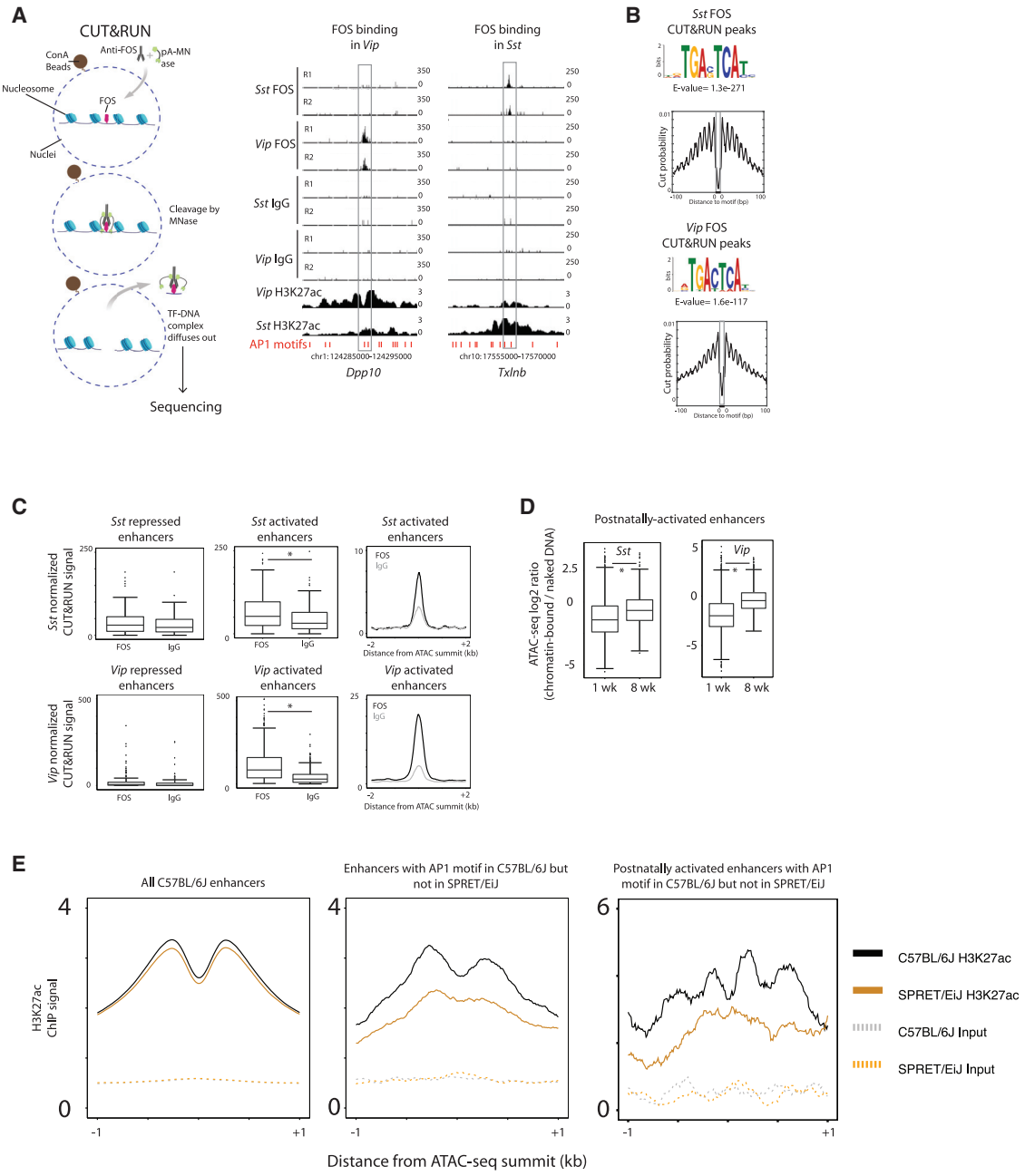

Figure 6. The Transcription Factor FOS Regulates Postnatally Activated Enhancers

(A) Scheme of FOS CUT&RUN. Figure was adapted from (Skene and Henikoff 2017; left). On the right are genome-browser views of FOS CUT&RUN data showing neuronal subtype-specific FOS binding sites at gene-distal genomic sites downstream of *Dpp10* (left) and *Txlnb* (right) genes. Two biological replicates of data are shown (R1 and R2).

(B) Footprints within FOS CUT&RUN peaks are enriched in AP1 binding motifs. AP1 binding motifs were the most significantly enriched motifs within the footprints (CutRunTools; Zhu et al., 2019), and distribution of nuclease cut probabilities surrounding the AP1 motifs is shown. The 10-bp periodicity flanking may reflect nucleosomes flanking the FOS binding sites, exposing DNA to MNase digestion every 10 bp.

(C) FOS is bound across postnatally activated enhancers. FOS CUT&RUN reads were quantified within postnatally repressed or activated enhancers (left and middle). The average distribution of FOS binding across the GREs within the postnatally activated enhancers is also shown (right). *p < 1e–9; Wilcoxon rank sum test.

(D) Postnatal increase in chromatin accessibility within postnatally activated enhancers. ATAC-seq read densities in *Sst* or *Vip* neurons were quantified within the regulatory regions of postnatally activated enhancers at postnatal 1 week and 8 weeks. The ratio of ATAC-seq read densities to genomic DNA transposed by the Tn5 transposase were plotted (see STAR Methods). *p < 1e–3; Wilcoxon rank sum test.

(legend continued on next page)

Please cite this article in press as: Stroud et al., An Activity-Mediated Transition in Transcription in Early Postnatal Neurons, Neuron (2020), https://doi.org/10.1016/j.neuron.2020.06.008

Sp8 in *Vip* neurons), in contrast to activity-dependent factors, such as FOS, the level of expression of these subtype-specific TFs does not increase during the time period during which postnatal enhancers are formed (Figure S6A). This suggests that these subtype-specific TFs, although possibly contributing to the selection of subtype-specific postnatal enhancers, likely do not on their own initiate the formation of these enhancers in the postnatal period.

We considered the possibility that the trigger for enhancer formation might be induction of activity-dependent FOS TFs that then work together with pre-existing subtype-specific TFs to select postnatal subtype-specific enhancers as neurons mature. Consistent with this possibility, we find that many postnatally activated enhancers that are specifically selected in either *Sst* or *Vip* neurons contain AP1 motifs (Figure S6F). Moreover, the FOS CUT&RUN analyses indicate that the enhancers postnatally formed in *Sst* neurons, but not in *Vip* neurons, are enriched in FOS binding relative to IgG signal in *Sst* neurons, but not in *Vip* neurons (Figures S6G and S6H). Likewise, enhancers formed in *Vip* neurons, but not in *Sst* neurons, selectively bind FOS in *Vip* neurons, but not in *Sst* neurons. These results indicate that FOS can bind to newly forming postnatal neuronal enhancers in a neuronal subtype-specific manner, consistent with the idea that the induction of FOS triggers the formation of these enhancers likely by cooperating with a neuronal subtype-specific TF that may be expressed prior to the induction of AP1 TFs.

We investigated the mechanism of enhancer activation during the postnatal period first by assessing whether the TF binding sites within these enhancers are already accessible prior to enhancer activation because of binding of a subtype-specific pioneer TF or whether these enhancers are initially occluded by nucleosomes that are then remodeled as the expression of AP1 factors is induced as a consequence of stimulation (Su et al., 2017). Quantification of ATAC-seq reads within these GREs indicates that these enhancers become more accessible as the brain matures in the postnatal period from 1 week to 8 weeks (Figure 6D), suggesting that the nucleosomes that occupy these regulatory regions are remodeled as neurons transition from an immature state to a mature state in early life.

A recent study in fibroblasts demonstrated that FOS-bound enhancers are occluded by nucleosomes prior to growth factor stimulation and that, upon stimulation, AP1 TFs recruit the SWI/SNF BAF chromatin complex that then remodels the enhancer, thus facilitating TF binding (Vierbuchen et al., 2017). To begin to test this model *in vivo*, we performed CUT&RUN using anti-ARID1A antibodies in *Sst* neurons. ARID1A is a canonical DNA-binding subunit of the SWI/SNF BAF complex (Son and Crabtree, 2014). We found that ARID1A binding is significantly enriched across FOS-binding sites, including those that reside within postnatally activated enhancers (Figures S6I–S6K). The postnatally induced enhancers lack ARID1A binding at 1 week when FOS is not bound to the enhancer sequences but co-acquire ARID1A and FOS binding by 3 weeks (Figures S6K–S6M). After 3 weeks, ARID1A, but not necessarily FOS, continues to bind to the postnatally activated enhancers throughout adulthood, likely maintaining the enhancers in an active state (Figures S6L and S6M). Therefore, our results suggest that postnatally activated neuronal enhancers are formed via AP1 TF recruitment of the SWI/SNF BAF complex. However, it remains possible that additional activity-dependent mechanisms, such as the post-translational modifications of TFs (Shalizi et al., 2006) and/or metabolic effects on chromatin structure (Li et al., 2018), also contribute to recruitment of the SWI/SNF BAF complex during postnatal neuronal enhancer formation.

An Unbiased Genetic Screen Reveals a Key Role for AP1 TFs in Controlling Postnatally Activated Enhancers *In Vivo*

To determine whether AP1 TFs are required for postnatal neuronal enhancer formation *in vivo* during early postnatal mouse brain development, we examined the effects of natural genetic variations in AP1 sites on enhancer activation (Vierbuchen et al., 2017). Comparison of the C57BL/6J and SPRET/EiJ genomes reveals $\sim$3.7 $\times$ 10^7 single-nucleotide polymorphisms (SNPs) across these two genomes, resulting in about one SNP per 80 bp of genomic sequence (Keane et al., 2011). If a SNP is present in an AP1 site within an enhancer and the SNP prevents binding of AP1, this should allow us to assess the requirement of FOS/JUN complexes for enhancer activation. To test whether AP1 TFs are important for postnatal enhancer activation in *Sst* neurons, we crossed *Sst-cre; Sun1* mice in the C57BL6 background with wild-type SPRET/EiJ mice (Figure 6E). We isolated *Sst*-expressing nuclei from cortices from 3-week-old F1 hybrid transgenic mice and performed H3K27ac ChIP-seq to generate allele-specific maps of enhancers in *Sst* neurons.

Quantification of H3K27ac levels at all C57BL6 enhancers for the C57BL6 and SPRET/EiJ alleles in *Sst*-expressing nuclei confirmed that the levels of H3K27ac are similar for both the C57BL6 and SPRET/EiJ alleles (Figure 6E). By contrast, when we focused the analysis on postnatally activated enhancers that possess an intact AP1 motif in the C57BL6 genome but no consensus AP1 motif in the SPRET/EiJ genome (Risse et al., 1989), we found that H3K27ac levels are reduced at these enhancers in the SPRET/EiJ allele compared to the C57BL6 allele. This suggests that mutation of the AP1 motif in SPRET/EiJ is associated with a decrease in the activity of the enhancer and that AP1 TFs contribute to the activation of postnatally induced enhancers *in vivo*.

AP1 TFs Control a Postnatally Activated Enhancer in an Activity-Dependent Manner

We investigated further whether AP1-TF-dependent postnatal neuronal enhancer activation is enhanced by neuronal activity. We focused our analyses on a postnatally activated enhancer cluster that lies 40 kb upstream of the *Igf1* gene and appears to function selectively in *Vip* neurons. The *Igf1* gene encodes a secreted factor that mediates activity-dependent inhibition of *Vip* neurons in the visual cortex and is required for normal visual

(E) Mutations in AP1 motifs are associated with decreased enhancer activity in *Sst* neurons. The distribution of H3K27ac in C57BL/6J and SPRET/EiJ alleles in Sst neurons of F1 hybrid mice was analyzed. H3K27ac and input DNA patterns were quantified across all C57BL/6J enhancers (left), all enhancers with intact AP1 motif in C57BL/6J that are mutated in SPRET/EiJ, and postnatally activated enhancers with intact AP1 motif in C57BL/6J that is mutated in SPRET/EiJ.

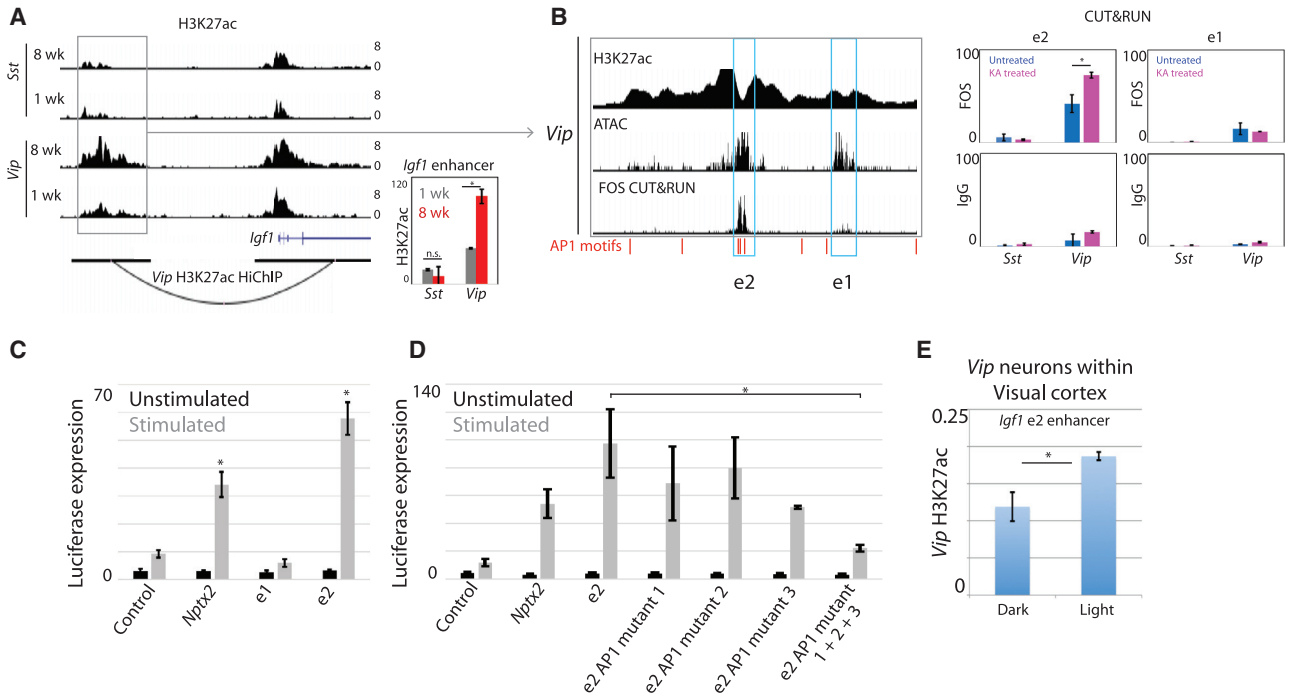

Figure 7. Neuronal Activity Modulates Postnatally Activated Enhancers

(A) Genome-browser view of the *Vip*-specific enhancer cluster upstream of the *Igf1* gene. Cortical H3K27ac ChIP and HiChIP data are shown. Quantification of H3K27ac within the *Igf1* enhancer in *Sst* and *Vip* neurons is also shown. Error bars represent SD between biological replicates. *p < 0.05; two-tailed t test.

(B) The *Igf1* enhancer in *Vip* neurons within the visual cortex contains two GREs, e1 and e2, of which e2 is bound by FOS *in vivo* in *Vip* neurons. Genome-browser views along with visual cortex ATAC-seq data are shown (left). We note that the ATAC-seq peaks were detected in the visual cortex, but not reproducibly detected across the whole cortex. Whole-cortex FOS and IgG CUT&RUN read densities were quantified within e1 and e2 (right). Error bars represent SD between biological replicates.

(C) *Igf1* e2 is induced by neuronal activity in an AP1-TF-dependent manner *in vitro*. Days *in vitro* (DIV) 7 mouse cortical neurons were stimulated by KCl treatment. "Control" represents the *Nptx2* reporter backbone without the *Nptx2* enhancer, and "*Nptx2*" represents the *Nptx2* reporter backbone, including the *Nptx2* enhancer (Malik et al., 2014). Luciferase expression was quantified by normalizing the firefly luciferase signal to Renilla luciferase signal from the same samples. Error bars represent SD between three independent experiments (biological replicates). *p < 0.05; two-tailed t test compared to control.

(D) *Igf1* e2 is activity induced in an AP1-dependent manner *in vitro*. Luciferase assays were analyzed as in (C). Error bars represent SD between three to five independent experiments (biological replicates). *p < 0.05; two-tailed t test.

(E) *Igf1* e2 is induced by visual stimulation in *Vip* neurons *in vivo*. H3K27ac ChIP-seq read densities within the e2 enhancer region from *Vip* neurons within visual cortices of mice either dark reared or light exposed were quantified. *p < 0.05; two-tailed t test.

acuity (Mardinly et al., 2016). Our *Vip* HiChIP experiments indicate that this enhancer cluster physically interacts with the promoter of the *Igf1* gene, suggesting that this enhancer cluster is a bona fide *Igf1* enhancer (Figure 7A). Notably, the *Igf1* enhancer is methylated at cytosines in the mouse cortex 1 week after birth in both *Sst* and *Vip* neurons but progressively becomes demethylated specifically in *Vip* neurons as they mature in the postnatal period (Figures S7A and S7B), suggesting that this enhancer is being activated in a neuronal subtype-specific manner.

We found by ATAC-seq of *Vip* neurons in the visual cortex that this enhancer contains two discrete regulatory regions: one of these elements (e1) lacks AP1 binding motifs, whereas the other (e2) contains three AP1 motifs (Figure 7B). Our cortical CUT&RUN analysis using anti-FOS antibodies suggested substantial binding of FOS to e2, but not to e1, in *Vip* neurons, but not *Sst* neurons, indicating that FOS may activate the *Igf1* gene in *Vip* neurons by selectively binding to e2 (Figure 7B).

To determine whether AP1 TFs mediate the induction of *Igf1* by binding to *Igf1* e2, we performed luciferase reporter assays in cortical neuron or caudal ganglionic eminence (CGE) cultures to assess whether the *Igf1* enhancer functions in an AP1-dependent manner. We cloned DNA sequences spanning *Igf1* e1 or e2, and versions of e2 in which the AP1 sites were mutated, into a luciferase reporter construct that contains the neuronal-activity-responsive pentraxin 2 (*Nptx2*) promoter (Malik et al., 2014). These reporter constructs were then transfected into embryonic cortical cultures, as well as CGE cultures, and the cultures were either left untreated or exposed to elevated levels of KCl at *in vitro* day 7 (DIV7), conditions that are known to activate calcium influx through L-type voltage-sensitive calcium channels and stimulate the production of AP1 TFs. In extracts from these cultures, we observe significant induction of luciferase activity selectively in membrane-depolarized neurons in which the wild-type *Igf1* e2 is cloned upstream of the luciferase gene (Figures 7C and S7C). By contrast, we observe only a low level of luciferase expression in the absence of membrane depolarization or in membrane-depolarized neurons in which the AP1 site-mutated e2 is driving luciferase expression (Figure 7D). In addition, we found that wild-type

Please cite this article in press as: Stroud et al., An Activity-Mediated Transition in Transcription in Early Postnatal Neurons, Neuron (2020), https://doi.org/10.1016/j.neuron.2020.06.008

Igf1 e1, which contains no AP1 sites, does not drive significant luciferase expression. These findings indicate that, during postnatal development, the binding of AP1 TFs to *Igf1* e2 contributes to postnatal e2 enhancer activation and activity-dependent *Igf1* transcription in *Vip* interneurons.

To consider further whether postnatal enhancers are formed/activated by neuronal activity *in vivo*, we examined whether these enhancers, and in particular *Igf1* e2, are activity regulated *in vivo*. *Vip*-cre; *Sun1* mice were dark reared and then we acutely exposed the mice to light (see STAR Methods). We isolated *Vip* nuclei from the visual cortices and performed H3K27ac ChIP-seq to generate genome-wide maps of light-induced enhancers. These enhancer maps were compared to those obtained from dark-reared mice. This analysis revealed that, in light exposed mice, there is a significant increase in the level of H3K27ac at the *Igf1* e2 enhancer (Figure 7E). These findings indicate that neuronal activity activates the *Igf1* e2 enhancer and likely other postnatally selected enhancers across the neuronal genome.

Neuronal Activity Modulates Postnatal Transitions in Neuronal Transcription States

To determine whether neuronal activity is required for the postnatal transition in gene expression, we reduced the activity of specific neuronal populations and assessed the effect on postnatal gene activation. We chose to silence *Sst* neurons, because previous studies had suggested that neuronal activity plays a critical role in the development of these neurons (Close et al., 2012; Denaxa et al., 2012). We generated adeno-associated viruses (AAVs) that express the inward rectifying potassium channel KIR2.1 in a Cre-dependent manner. KIR2.1 overexpression is a well-established method for reducing neuronal activity (Wiegert et al., 2017). As a control, we also generated AAVs that express a mutated form of KIR2.1 that make non-conducting channels (Xue et al., 2014). We injected P1 *Sst*-cre; *Sun1* mice with either the KIR2.1 AAVs or mutated KIR2.1 AAVs (KIR2.1mut) and collected cortices at 7 weeks (Figure S7D). To enrich for the sparsely infected *Sst* neurons, we FACS sorted using the GFP epitope of the SUN1 construct and then performed high-throughput single-nuclei sequencing on the FACS-sorted *Sst* nuclei (Figure S7E). To enable robust detection of viral transcripts in our analyses, we enriched for the viral transcripts by PCR (see STAR Methods). Through this approach, we were able to distinguish *Sst* nuclei that were infected and express the viral transcripts from *Sst* nuclei that were not infected. Altogether, we obtained more than 700 high-quality nuclei for each of KIR2.1-infected and KIR2.1mut-infected samples.

When all genes were analyzed in aggregate, we observed no change in overall gene expression between KIR2.1- and KIR2.1-mut-expressing neurons, indicating that the presence of the active KIR2.1 channel does not have a deleterious effect on *Sst* neuron health (Figure S7F). When we analyzed the set of genes that are known to be induced upon visual stimulation of dark-reared mice (Mardinly et al., 2016), we found that the genes that are upregulated by visual stimulation are downregulated in the KIR2.1-expressing neurons relative to the KIR2.1mut-expressing neurons (Figure S7F). As a control in this experiment, we examined gene expression in the AAV-uninfected subset of *Sst* neurons obtained from the brains of mice infected with the KIR2.1 or KIR2.1mut viruses. In this case, we observed no significant changes in expression of the light-induced genes (Figure S7F). This suggests that the overexpression of KIR2.1 leads to a decrease in the expression of activity-regulated genes selectively in infected *Sst* neurons.

Between KIR2.1- and KIR2.1mut-expressing nuclei, we identified 264 genes that are significantly downregulated in KIR2.1 compared to KIR2.1mut ($p < 0.05$). We note that the degree of reduction in gene expression upon KIR2.1 overexpression is modest (possibly due to homeostatic responses that compensate when the activity of the neuron is blocked), and therefore, we may be capturing only a subset of genes that are regulated by neuronal activity in these neurons. Nevertheless, by comparing this subset of activity-induced genes to the postnatally inducible gene set, we find a statistically significant overlap between the activity-regulated genes and postnatally inducible genes ($p = 4 \times 10^{-5}$; Figures S7G and S7H). This subset of genes includes *Etl4*/*Skt*, a gene required for intervertebral disk development (Semba et al., 2006). Notably, H3K27ac HiChIP and anti-FOS CUT&RUN analyses in *Sst* neurons indicate that the *Etl4* promoter interacts with multiple gene-distal postnatally formed enhancers, including one that is bound by FOS, suggesting the possibility that, during early life, FOS contributes to the formation and/or activation of new enhancers in an activity-dependent manner, which then mediate an increase in activity-dependent gene transcription (Figure S7I). Finally, we note that there is heterogeneity across different tentative subclasses of *Sst* neurons in the degree of downregulated expression of postnatally induced genes upon KIR2.1 overexpression (Figure S7J).

DISCUSSION

During early life, postmitotic neurons continue to acquire morphological and functional properties that are essential for proper brain function. In this study, we identify gene-regulatory programs that contribute to early postnatal brain maturation, and we identify activity-regulated AP1 TFs as key mediators of this maturation process. As neurons mature, the expression of AP1 TFs is activated and is correlated with the formation of new gene-distal enhancers that increase the expression of sets of genes that include neuron-subtype-specific genes.

We also find that a major feature of postnatal neuronal maturation is the widespread decommissioning of enhancers that drive expression of cell proliferation and migration genes during earlier stages of brain development. Interestingly, early differentiation programs are not completely turned off until 3 weeks after birth. This suggests that immature neurons in the early postnatal mouse brain retain a transcriptional memory of earlier stages of neuronal development. The repression of embryonic enhancers occurs at the same time that DNMT3A catalyzes methylation at cytosines in the postnatal brain (Lister et al., 2013; Stroud et al., 2017). Mutations in DNMT3A are found in individuals with autism and intellectual disabilities, suggesting an essential role for DNMT3A in normal nervous system development and function (Sanders et al., 2015; Tatton-Brown et al., 2014). The majority of methylation deposited at this stage occurs at CA sequences, and CA methylation across gene bodies appears to function in neuronal subtype-specific fine-tuning of gene

Please cite this article in press as: Stroud et al., An Activity-Mediated Transition in Transcription in Early Postnatal Neurons, Neuron (2020), https://doi.org/10.1016/j.neuron.2020.06.008

transcription (Lavery et al., 2020; Mo et al., 2015; Stroud et al., 2017; Li et al., 2019). In agreement with Li et al., 2019, we show here that, during the early postnatal period, DNMT3A also methylates CG sequences within various enhancers across the genome, including those that drive embryonic gene expression, thus in part contributing to embryonic enhancer silencing in the postnatal period. Interestingly, we find that neuronal subtype-specific deletions of DNMT3A in either *Sst* or *Vip* neurons result in mild activation of embryonic enhancers in adult brains, suggesting that adult *Dnmt3a* KO neurons are in part in an immature state compared to adult wild-type neurons. Hence, a failure to shut down embryonic enhancers may in part underlie neuronal defects observed in individuals bearing DNMT3A mutations or mutations in MECP2 (e.g., in Rett syndrome), which binds these enhancers once they are methylated.

Neuronal activity is usually thought to be associated with transient neuronal processes (Yap and Greenberg, 2018). Here, we find that, as neurons mature, AP1 TFs are persistently expressed at higher levels and regulate the formation of enhancers that in turn increase the expression of key neuronal maturation genes. Although it is well known that AP1 TFs can be rapidly and transiently activated by neuronal activity in the mature brain throughout life, the importance for AP1 TFs in brain maturation and function was poorly understood (Yap and Greenberg, 2018). The genome-wide analysis of FOS binding in the cortex described here suggests that a previously unappreciated function of FOS is as a mediator of the activation of postnatal neuronal enhancers in early life that control the maturation of cortical circuits. Rather than activating pre-specified subsets of poised enhancers, we find that *de novo* formation of enhancers occurs during neuronal maturation in the postnatal period. This suggests that the selection of neuronal subtype-specific enhancers occurs as neurons interact with other cells in their local microenvironment and as animals receive sensory input from their external environment in early life. Because AP1 TFs are induced by neuronal activity across essentially all neuronal subtypes (Hrvatin et al., 2018), it is likely that we have uncovered a general mechanism by which gene expression is regulated in many types of neurons in the postnatal period. We note that, in addition to being activated by neuronal activity, AP1 TFs are also induced in response to other external stimuli, such as growth factors (Greenberg and Ziff, 1984), and therefore, it is likely that other extracellular factors also contribute to the process of enhancer-dependent neuronal differentiation and maturation (Kim et al., 2010).

Regulatory Approval

All experiments were performed following procedures approved by the Harvard Medical Area Standing Committee on Animals (HMA IACUC).

STAR★METHODS

Detailed methods are provided in the online version of this paper and include the following:

SUPPLEMENTAL INFORMATION

Supplemental Information can be found online at https://doi.org/10.1016/j.neuron.2020.06.008.

ACKNOWLEDGMENTS

We thank the members of the Greenberg laboratory for helpful discussions; P. Zhang for assistance in maintenance of the mouse colony; K. Mei and G. Boulting for advice on CGE dissections and luciferase experiments; and G. Fishell, C. Harwell, E. Griffith, S. Ashrafi, and E. Pollina for editorial assistance. This work was supported by grants from the Rett Syndrome Research Trust and the NIH (1RO1NS048276) to M.E.G. C.P.D. was supported by NIH grants T32-NS007473 and F32-NS112455. M.G.Y. was supported by NIH grant T32EY007110. M.A.S. was supported by NIH grant U01MH106883 and the MIT Jarve Seed Fund for Science Innovation. H.S. was supported by NARSAD and Damon Runyon and Charles A. King Trust fellowships.

AUTHOR CONTRIBUTIONS

H.S. conceived the study. H.S., Y.N.T., and C.P.D. performed the experiments. H.S., M.G.Y., Y.N.T., M.S., S.H., and M.E.G. analyzed the data. E.L. contributed essential reagents. H.S. and M.E.G. wrote the paper.

DECLARATION OF INTERESTS

The authors declare no competing interests.

Received: July 30, 2019
Revised: March 31, 2020
Accepted: June 4, 2020
Published: June 25, 2020

SUPPORTING CITATIONS

The following references appear in the Supplemental Information: Finucane et al. (2018); Gazal et al. (2017); Rizzardi et al. (2019); Shen et al. (2012).

REFERENCES

Alitto, H.J., and Dan, Y. (2013). Cell-type-specific modulation of neocortical activity by basal forebrain input. Front. Syst. Neurosci. *6*, 79.

Altshuler, D.M., Gibbs, R.A., Peltonen, L., Altshuler, D.M., Gibbs, R.A., Peltonen, L., Dermitzakis, E., Schaffner, S.F., Yu, F., Peltonen, L., et al.; International HapMap 3 Consortium (2010). Integrating common and rare genetic variation in diverse human populations. Nature *467*, 52–58.

Anders, S., Pyl, P.T., and Huber, W. (2015). HTSeq–a Python framework to work with high-throughput sequencing data. Bioinformatics *31*, 166–169.

Bailey, T.L., and Machanick, P. (2012). Inferring direct DNA binding from ChIP-seq. Nucleic Acids Res. *40*, e128.

Bailey, T.L., Boden, M., Buske, F.A., Frith, M., Grant, C.E., Clementi, L., Ren, J., Li, W.W., and Noble, W.S. (2009). MEME SUITE: tools for motif discovery and searching. Nucleic Acids Res. *37*, W202–W208.

Berry, K.P., and Nedivi, E. (2016). Experience-dependent structural plasticity in the visual system. Annu. Rev. Vis. Sci. *2*, 17–35.

Bipolar Disorder and Schizophrenia Working Group of the Psychiatric Genomics Consortium (2018). Genomic dissection of bipolar disorder and schizophrenia, including 28 subphenotypes. Cell *173*, 1705–1715.e16.

Bolger, A.M., Lohse, M., and Usadel, B. (2014). Trimmomatic: a flexible trimmer for Illumina sequence data. Bioinformatics *30*, 2114–2120.

Buenrostro, J.D., Giresi, P.G., Zaba, L.C., Chang, H.Y., and Greenleaf, W.J. (2013). Transposition of native chromatin for fast and sensitive epigenomic profiling of open chromatin, DNA-binding proteins and nucleosome position. Nat. Methods *10*, 1213–1218.

Calo, E., and Wysocka, J. (2013). Modification of enhancer chromatin: what, how, and why? Mol. Cell *49*, 825–837.

Chahrour, M., and Zoghbi, H.Y. (2007). The story of Rett syndrome: from clinic to neurobiology. Neuron *56*, 422–437.

Chen, W.G., Chang, Q., Lin, Y., Meissner, A., West, A.E., Griffith, E.C., Jaenisch, R., and Greenberg, M.E. (2003). Derepression of BDNF transcription involves calcium-dependent phosphorylation of MeCP2. Science *302*, 885–889.

Chen, L.F., Zhou, A.S., and West, A.E. (2017). Transcribing the connectome: roles for transcription factors and chromatin regulators in activity-dependent synapse development. J. Neurophysiol. *118*, 755–770.

Clemens, A.W., Wu, D.Y., Moore, J.R., Christian, D.L., Zhao, G., and Gabel, H.W. (2020). MeCP2 represses enhancers through chromosome topology-associated DNA methylation. Mol. Cell *77*, 279–293.e8.

Close, J., Xu, H., De Marco García, N., Batista-Brito, R., Rossignol, E., Rudy, B., and Fishell, G. (2012). Satb1 is an activity-modulated transcription factor required for the terminal differentiation and connectivity of medial ganglionic eminence-derived cortical interneurons. J. Neurosci. *32*, 17690–17705.

Conti, F., Minelli, A., and Melone, M. (2004). GABA transporters in the mammalian cerebral cortex: localization, development and pathological implications. Brain Res. Brain Res. Rev. *45*, 196–212.

Denaxa, M., Kalaitzidou, M., Garefalaki, A., Achimastou, A., Lasrado, R., Maes, T., and Pachnis, V. (2012). Maturation-promoting activity of SATB1 in MGE-derived cortical interneurons. Cell Rep. *2*, 1351–1362.

Fernandez-Albert, J., Lipinski, M., Lopez-Cascales, M.T., Rowley, M.J., Martin-Gonzalez, A.M., Del Blanco, B., Corces, V.G., and Barco, A. (2019). Immediate and deferred epigenomic signatures of in vivo neuronal activation in mouse hippocampus. Nat. Neurosci. *22*, 1718–1730.

Finucane, H.K., Bulik-Sullivan, B., Gusev, A., Trynka, G., Reshef, Y., Loh, P.R., Anttila, V., Xu, H., Zang, C., Farh, K., et al.; ReproGen Consortium; Schizophrenia Working Group of the Psychiatric Genomics Consortium; RACI Consortium (2015). Partitioning heritability by functional annotation using genome-wide association summary statistics. Nat. Genet. *47*, 1228–1235.

Finucane, H.K., Reshef, Y.A., Anttila, V., Slowikowski, K., Gusev, A., Byrnes, A., Gazal, S., Loh, P.R., Lareau, C., Shoresh, N., et al.; Brainstorm Consortium (2018). Heritability enrichment of specifically expressed genes identifies disease-relevant tissues and cell types. Nat. Genet. *50*, 621–629.

Fiumelli, H., Cancedda, L., and Poo, M.M. (2005). Modulation of GABAergic transmission by activity via postsynaptic Ca2+-dependent regulation of KCC2 function. Neuron *48*, 773–786.

Flint, A.C., Maisch, U.S., Weishaupt, J.H., Kriegstein, A.R., and Monyer, H. (1997). NR2A subunit expression shortens NMDA receptor synaptic currents in developing neocortex. J. Neurosci. *17*, 2469–2476.

Frank, C.L., Liu, F., Wijayatunge, R., Song, L., Biegler, M.T., Yang, M.G., Vockley, C.M., Safi, A., Gersbach, C.A., Crawford, G.E., and West, A.E. (2015). Regulation of chromatin accessibility and Zic binding at enhancers in the developing cerebellum. Nat. Neurosci. *18*, 647–656.

Gazal, S., Finucane, H.K., Furlotte, N.A., Loh, P.R., Palamara, P.F., Liu, X., Schoech, A., Bulik-Sullivan, B., Neale, B.M., Gusev, A., and Price, A.L. (2017). Linkage disequilibrium-dependent architecture of human complex traits shows action of negative selection. Nat. Genet. *49*, 1421–1427.

Greenberg, M.E., and Ziff, E.B. (1984). Stimulation of 3T3 cells induces transcription of the c-fos proto-oncogene. Nature *311*, 433–438.

Grove, J., Ripke, S., Als, T.D., Mattheisen, M., Walters, R.K., Won, H., Pallesen, J., Agerbo, E., Andreassen, O.A., Anney, R., et al.; Autism Spectrum Disorder Working Group of the Psychiatric Genomics Consortium; BUPGEN; Major Depressive Disorder Working Group of the Psychiatric Genomics Consortium; 23andMe Research Team (2019). Identification of common genetic risk variants for autism spectrum disorder. Nat. Genet. *51*, 431–444.

Guy, J., Hendrich, B., Holmes, M., Martin, J.E., and Bird, A. (2001). A mouse Mecp2-null mutation causes neurological symptoms that mimic Rett syndrome. Nat. Genet. *27*, 322–326.

Hainer, S.J., and Fazzio, T.G. (2019). High-resolution chromatin profiling using CUT&RUN. Curr. Protoc. Mol. Biol. *126*, e85.

Harris, J.A., Hirokawa, K.E., Sorensen, S.A., Gu, H., Mills, M., Ng, L.L., Bohn, P., Mortrud, M., Ouellette, B., Kidney, J., et al. (2014). Anatomical characterization of Cre driver mice for neural circuit mapping and manipulation. Front. Neural Circuits *8*, 76.

Heintzman, N.D., Hon, G.C., Hawkins, R.D., Kheradpour, P., Stark, A., Harp, L.F., Ye, Z., Lee, L.K., Stuart, R.K., Ching, C.W., et al. (2009). Histone modifications at human enhancers reflect global cell-type-specific gene expression. Nature *459*, 108–112.

Heinz, S., Benner, C., Spann, N., Bertolino, E., Lin, Y.C., Laslo, P., Cheng, J.X., Murre, C., Singh, H., and Glass, C.K. (2010). Simple Combinations of Lineage-Determining Transcription Factors Prime Cis-Regulatory Elements Required for Macrophage and B Cell Identities. Mol. Cell *38*, 576–589.

Hrvatin, S., Hochbaum, D.R., Nagy, M.A., Cicconet, M., Robertson, K., Cheadle, L., Zilionis, R., Ratner, A., Borges-Monroy, R., Klein, A.M., et al. (2018). Single-cell analysis of experience-dependent transcriptomic states in the mouse visual cortex. Nat. Neurosci. *21*, 120–129.

Hu, P., Fabyanic, E., Kwon, D.Y., Tang, S., Zhou, Z., and Wu, H. (2017). Dissecting cell-type composition and activity-dependent transcriptional state in mammalian brains by massively parallel single-nucleus RNA-seq. Mol. Cell *68*, 1006–1015.e7.

Huang, D.W., Sherman, B.T., and Lempicki, R.A. (2009). Systematic and integrative analysis of large gene lists using DAVID bioinformatics resources. Nat. Protoc. *4*, 44–57.

Huang, S., Holt, J., Kao, C.Y., McMillan, L., and Wang, W. (2014). A novel multi-alignment pipeline for high-throughput sequencing data. Database (Oxford) *2014*, bau057.

Javierre, B.M., Burren, O.S., Wilder, S.P., Kreuzhuber, R., Hill, S.M., Sewitz, S., Cairns, J., Wingett, S.W., Várnai, C., Thiecke, M.J., et al. (2016). Lineage-specific genome architecture links enhancers and non-coding disease variants to target gene promoters. Cell *167*, 1369–1384.e19.

Kaneda, M., Okano, M., Hata, K., Sado, T., Tsujimoto, N., Li, E., and Sasaki, H. (2004). Essential role for de novo DNA methyltransferase Dnmt3a in paternal and maternal imprinting. Nature *429*, 900–903.

Keane, T.M., Goodstadt, L., Danecek, P., White, M.A., Wong, K., Yalcin, B., Heger, A., Agam, A., Slater, G., Goodson, M., et al. (2011). Mouse genomic variation and its effect on phenotypes and gene regulation. Nature *477*, 289–294.

Kessaris, N., Magno, L., Rubin, A.N., and Oliveira, M.G. (2014). Genetic programs controlling cortical interneuron fate. Curr. Opin. Neurobiol. *26*, 79–87.

Kim, T.K., Hemberg, M., Gray, J.M., Costa, A.M., Bear, D.M., Wu, J., Harmin, D.A., Laptewicz, M., Barbara-Haley, K., Kuersten, S., et al. (2010). Widespread transcription at neuronal activity-regulated enhancers. Nature *465*, 182–187.

Kim, D., Pertea, G., Trapnell, C., Pimentel, H., Kelley, R., and Salzberg, S.L. (2013). TopHat2: accurate alignment of transcriptomes in the presence of insertions, deletions and gene fusions. Genome Biol. *14*, R36.

Krashes, M.J., Koda, S., Ye, C., Rogan, S.C., Adams, A.C., Cusher, D.S., Maratos-Flier, E., Roth, B.L., and Lowell, B.B. (2011). Rapid, Reversible Activation of AgRP Neurons Drives Feeding Behavior in Mice. J. Clin. Invest. *121*, 1424–1428.

Lacar, B., Linker, S.B., Jaeger, B.N., Krishnaswami, S.R., Barron, J.J., Kelder, M.J.E., Parylak, S.L., Paquola, A.C.M., Venepally, P., Novotny, M., et al. (2016). Nuclear RNA-seq of single neurons reveals molecular signatures of activation. Nat. Commun. *7*, 11022.

Landt, S.G., Marinov, G.K., Kundaje, A., Kheradpour, P., Pauli, F., Batzoglou, S., Bernstein, B.E., Bickel, P., Brown, J.B., Cayting, P., et al. (2012). ChIP-seq guidelines and practices of the ENCODE and modENCODE consortia. Genome Res. *22*, 1813–1831.

Langmead, B., Trapnell, C., Pop, M., and Salzberg, S.L. (2009). Ultrafast and memory-efficient alignment of short DNA sequences to the human genome. Genome Biol. *10*, R25.

Lareau, C.A., and Aryee, M.J. (2018). hichipper: a preprocessing pipeline for calling DNA loops from HiChIP data. Nat. Methods *15*, 155–156.

Lavery, L.A., Ure, K., Wan, Y.W., Luo, C., Trostle, A.J., Wang, W., Jin, H., Lopez, J., Lucero, J., Durham, M.A., et al. (2020). Losing Dnmt3a dependent methylation in inhibitory neurons impairs neural function by a mechanism impacting Rett syndrome. eLife *9*, e52981.

Le Magueresse, C., and Monyer, H. (2013). GABAergic interneurons shape the functional maturation of the cortex. Neuron *77*, 388–405.

Li, H., Handsaker, B., Wysoker, A., Fennell, T., Ruan, J., Homer, N., Marth, G., Abecasis, G., and Durbin, R.; 1000 Genome Project Data Processing Subgroup (2009). The Sequence Alignment/Map format and SAMtools. Bioinformatics *25*, 2078–2079.

Li, X., Egervari, G., Wang, Y., Berger, S.L., and Lu, Z. (2018). Regulation of chromatin and gene expression by metabolic enzymes and metabolites. Nat. Rev. Mol. Cell Biol. *19*, 563–578.

Li, J., Pinto-Duarte, A., Zander, M., Lai, C., Osteen, J., Fang, L., Luo, C., Lucero, J.D., Gomez-Castanon, R., Nery, J.R., et al. (2019). Polycomb-mediated repression compensates for loss of postnatal DNA methylation in excitatory neurons. bioRxiv. https://doi.org/10.1101/2019.12.20.883694.

Lister, R., Mukamel, E.A., Nery, J.R., Urich, M., Puddifoot, C.A., Johnson, N.D., Lucero, J., Huang, Y., Dwork, A.J., Schultz, M.D., et al. (2013). Global epigenomic reconfiguration during mammalian brain development. Science *341*, 1237905.

Loh, P.R., Kichaev, G., Gazal, S., Schoech, A.P., and Price, A.L. (2018). Mixed-model association for biobank-scale datasets. Nat. Genet. *50*, 906–908.

Love, M.I., Huber, W., and Anders, S. (2014). Moderated estimation of fold change and dispersion for RNA-seq data with DESeq2. Genome Biol. *15*, 550.

Lyst, M.J., Ekiert, R., Ebert, D.H., Merusi, C., Nowak, J., Selfridge, J., Guy, J., Kastan, N.R., Robinson, N.D., de Lima Alves, F., et al. (2013). Rett syndrome mutations abolish the interaction of MeCP2 with the NCoR/SMRT co-repressor. Nat. Neurosci. *16*, 898–902.

Malik, A.N., Vierbuchen, T., Hemberg, M., Rubin, A.A., Ling, E., Couch, C.H., Stroud, H., Spiegel, I., Farh, K.K., Harmin, D.A., and Greenberg, M.E. (2014). Genome-wide identification and characterization of functional neuronal activity-dependent enhancers. Nat. Neurosci. *17*, 1330–1339.

Mardinly, A.R., Spiegel, I., Patrizi, A., Centofante, E., Bazinet, J.E., Tzeng, C.P., Mandel-Brehm, C., Harmin, D.A., Adesnik, H., Fagiolini, M., and Greenberg, M.E. (2016). Sensory experience regulates cortical inhibition by inducing IGF1 in VIP neurons. Nature *531*, 371–375.

Marín, O. (2016). Developmental timing and critical windows for the treatment of psychiatric disorders. Nat. Med. *22*, 1229–1238.

Martin, J., Walters, R.K., Demontis, D., Mattheisen, M., Lee, S.H., Robinson, E., Brikell, I., Ghirardi, L., Larsson, H., Lichtenstein, P., et al.; 23andMe Research Team; Psychiatric Genomics Consortium: ADHD Subgroup; iPSYCH–Broad ADHD Workgroup (2018). A genetic investigation of sex bias in the prevalence of attention-deficit/hyperactivity disorder. Biol. Psychiatry *83*, 1044–1053.

McLean, C.Y., Bristor, D., Hiller, M., Clarke, S.L., Schaar, B.T., Lowe, C.B., Wenger, A.M., and Bejerano, G. (2010). GREAT improves functional interpretation of cis-regulatory regions. Nat. Biotechnol. *28*, 495–501.

Mifsud, B., Tavares-Cadete, F., Young, A.N., Sugar, R., Schoenfelder, S., Ferreira, L., Wingett, S.W., Andrews, S., Grey, W., Ewels, P.A., et al. (2015). Mapping long-range promoter contacts in human cells with high-resolution capture Hi-C. Nat. Genet. *47*, 598–606.

Miyoshi, G., and Fishell, G. (2011). GABAergic interneuron lineages selectively sort into specific cortical layers during early postnatal development. Cereb. Cortex *21*, 845–852.

Mo, A., Mukamel, E.A., Davis, F.P., Luo, C., Henry, G.L., Picard, S., Urich, M.A., Nery, J.R., Sejnowski, T.J., Lister, R., et al. (2015). Epigenomic signatures of neuronal diversity in the mammalian brain. Neuron *86*, 1369–1384.

Molyneaux, B.J., Arlotta, P., Menezes, J.R., and Macklis, J.D. (2007). Neuronal subtype specification in the cerebral cortex. Nat. Rev. Neurosci. *8*, 427–437.

Mumbach, M.R., Rubin, A.J., Flynn, R.A., Dai, C., Khavari, P.A., Greenleaf, W.J., and Chang, H.Y. (2016). HiChIP: efficient and sensitive analysis of protein-directed genome architecture. Nat. Methods *13*, 919–922.

Mumbach, M.R., Satpathy, A.T., Boyle, E.A., Dai, C., Gowen, B.G., Cho, S.W., Nguyen, M.L., Rubin, A.J., Granja, J.M., Kazane, K.R., et al. (2017). Enhancer connectome in primary human cells identifies target genes of disease-associated DNA elements. Nat. Genet. *49*, 1602–1612.

Nord, A.S., Blow, M.J., Attanasio, C., Akiyama, J.A., Holt, A., Hosseini, R., Phouanenavong, S., Plajzer-Frick, I., Shoukry, M., Afzal, V., et al. (2013). Rapid and pervasive changes in genome-wide enhancer usage during mammalian development. Cell *155*, 1521–1531.

Okada, Y., Wu, D., Trynka, G., Raj, T., Terao, C., Ikari, K., Kochi, Y., Ohmura, K., Suzuki, A., Yoshida, S., et al.; RACI consortium; GARNET consortium (2014). Genetics of rheumatoid arthritis contributes to biology and drug discovery. Nature *506*, 376–381.

Ostuni, R., Piccolo, V., Barozzi, I., Polletti, S., Termanini, A., Bonifacio, S., Curina, A., Prosperini, E., Ghisletti, S., and Natoli, G. (2013). Latent enhancers activated by stimulation in differentiated cells. Cell *152*, 157–171.

Paul, A., Crow, M., Raudales, R., He, M., Gillis, J., and Huang, Z.J. (2017). Transcriptional architecture of synaptic communication delineates GABAergic neuron identity. Cell *171*, 522–539.e20.

Pfeffer, C.K., Xue, M., He, M., Huang, Z.J., and Scanziani, M. (2013). Inhibition of inhibition in visual cortex: the logic of connections between molecularly distinct interneurons. Nat. Neurosci. *16*, 1068–1076.

Reilly, S.K., Yin, J., Ayoub, A.E., Emera, D., Leng, J., Cotney, J., Sarro, R., Rakic, P., and Noonan, J.P. (2015). Evolutionary genomics. Evolutionary

changes in promoter and enhancer activity during human corticogenesis. Science *347*, 1155–1159.

Risse, G., Jooss, K., Neuberg, M., Brüller, H.J., and Müller, R. (1989). Asymmetrical recognition of the palindromic AP1 binding site (TRE) by Fos protein complexes. EMBO J. *8*, 3825–3832.

Rizzardi, L.F., Hickey, P.F., Rodriguez DiBlasi, V., Tryggvadóttir, R., Callahan, C.M., Idrizi, A., Hansen, K.D., and Feinberg, A.P. (2019). Neuronal brain-region-specific DNA methylation and chromatin accessibility are associated with neuropsychiatric trait heritability. Nat. Neurosci. *22*, 307–316.

Robinson, M.D., McCarthy, D.J., and Smyth, G.K. (2010). edgeR: a Bioconductor package for differential expression analysis of digital gene expression data. Bioinformatics *26*, 139–140.

Sanders, S.J., He, X., Willsey, A.J., Ercan-Sencicek, A.G., Samocha, K.E., Cicek, A.E., Murtha, M.T., Bal, V.H., Bishop, S.L., Dong, S., et al.; Autism Sequencing Consortium (2015). Insights into autism spectrum disorder genomic architecture and biology from 71 risk loci. Neuron *87*, 1215–1233.

Satija, R., Farrell, J.A., Gennert, D., Schier, A.F., and Regev, A. (2015). Spatial reconstruction of single-cell gene expression data. Nat. Biotechnol. *33*, 495–502.

Schizophrenia Working Group of the Psychiatric Genomics Consortium (2014). Biological insights from 108 schizophrenia-associated genetic loci. Nature *511*, 421–427.

Semba, K., Araki, K., Li, Z., Matsumoto, K., Suzuki, M., Nakagata, N., Takagi, K., Takeya, M., Yoshinobu, K., Araki, M., et al. (2006). A novel murine gene, Sickle tail, linked to the Danforth's short tail locus, is required for normal development of the intervertebral disc. Genetics *172*, 445–456.

Servant, N., Varoquaux, N., Lajoie, B.R., Viara, E., Chen, C.J., Vert, J.P., Heard, E., Dekker, J., and Barillot, E. (2015). HiC-Pro: an optimized and flexible pipeline for Hi-C data processing. Genome Biol. *16*, 259.

Shalizi, A., Gaudillière, B., Yuan, Z., Stegmüller, J., Shirogane, T., Ge, Q., Tan, Y., Schulman, B., Harper, J.W., and Bonni, A. (2006). A calcium-regulated MEF2 sumoylation switch controls postsynaptic differentiation. Science *311*, 1012–1017.

Shen, Y., Yue, F., McCleary, D.F., Ye, Z., Edsall, L., Kuan, S., Wagner, U., Dixon, J., Lee, L., Lobanenkov, V.V., and Ren, B. (2012). A map of the cis-regulatory sequences in the mouse genome. Nature *488*, 116–120.

Sheng, M., Cummings, J., Roldan, L.A., Jan, Y.N., and Jan, L.Y. (1994). Changing subunit composition of heteromeric NMDA receptors during development of rat cortex. Nature *368*, 144–147.

Skene, P.J., and Henikoff, S. (2017). An efficient targeted nuclease strategy for high-resolution mapping of DNA binding sites. eLife *6*, e21856.

Skene, P.J., Illingworth, R.S., Webb, S., Kerr, A.R., James, K.D., Turner, D.J., Andrews, R., and Bird, A.P. (2010). Neuronal MeCP2 is expressed at near histone-octamer levels and globally alters the chromatin state. Mol. Cell *37*, 457–468.

Son, E.Y., and Crabtree, G.R. (2014). The role of BAF (mSWI/SNF) complexes in mammalian neural development. Am. J. Med. Genet. C. Semin. Med. Genet. *166C*, 333–349.

Spitzer, N.C. (2017). Neurotransmitter switching in the developing and adult brain. Annu. Rev. Neurosci. *40*, 1–19.

Stroud, H., Su, S.C., Hrvatin, S., Greben, A.W., Renthal, W., Boxer, L.D., Nagy, M.A., Hochbaum, D.R., Kinde, B., Gabel, H.W., et al. (2017). Early-life gene expression in neurons modulates lasting epigenetic states. Cell *171*, 1151–1164.e16.

Su, Y., Shin, J., Zhong, C., Wang, S., Roychowdhury, P., Lim, J., Kim, D., Ming, G.L., and Song, H. (2017). Neuronal activity modifies the chromatin accessibility landscape in the adult brain. Nat. Neurosci. *20*, 476–483.

Sun, D., Xi, Y., Rodriguez, B., Park, H.J., Tong, P., Meong, M., Goodell, M.A., and Li, W. (2014). MOABS: model based analysis of bisulfite sequencing data. Genome Biol. *15*, R38.

Taniguchi, H., He, M., Wu, P., Kim, S., Paik, R., Sugino, K., Kvitsiani, D., Fu, Y., Lu, J., Lin, Y., et al. (2011). A resource of Cre driver lines for genetic targeting of GABAergic neurons in cerebral cortex. Neuron *71*, 995–1013.

Tatton-Brown, K., Seal, S., Ruark, E., Harmer, J., Ramsay, E., Del Vecchio Duarte, S., Zachariou, A., Hanks, S., O'Brien, E., Aksglaede, L., et al.; Childhood Overgrowth Consortium (2014). Mutations in the DNA methyltransferase gene DNMT3A cause an overgrowth syndrome with intellectual disability. Nat. Genet. *46*, 385–388.

Trapnell, C., Cacchiarelli, D., Grimsby, J., Pokharel, P., Li, S., Morse, M., Lennon, N.J., Livak, K.J., Mikkelsen, T.S., and Rinn, J.L. (2014). The dynamics and regulators of cell fate decisions are revealed by pseudotemporal ordering of single cells. Nat. Biotechnol. *32*, 381–386.

Tronche, F., Kellendonk, C., Kretz, O., Gass, P., Anlag, K., Orban, P.C., Bock, R., Klein, R., and Schütz, G. (1999). Disruption of the glucocorticoid receptor gene in the nervous system results in reduced anxiety. Nat. Genet. *23*, 99–103.

Urban-Ciecko, J., and Barth, A.L. (2016). Somatostatin-expressing neurons in cortical networks. Nat. Rev. Neurosci. *17*, 401–409.

Vierbuchen, T., Ling, E., Cowley, C.J., Couch, C.H., Wang, X., Harmin, D.A., Roberts, C.W.M., and Greenberg, M.E. (2017). AP-1 transcription factors and the BAF complex mediate signal-dependent enhancer selection. Mol. Cell *68*, 1067–1082.e12.

Visel, A., Taher, L., Girgis, H., May, D., Golonzhka, O., Hoch, R.V., McKinsey, G.L., Pattabiraman, K., Silberberg, S.N., Blow, M.J., et al. (2013). A high-resolution enhancer atlas of the developing telencephalon. Cell *152*, 895–908.

Wiegert, J.S., Mahn, M., Prigge, M., Printz, Y., and Yizhar, O. (2017). Silencing neurons: tools, applications, and experimental constraints. Neuron *95*, 504–529.

Wiesel, T.N., and Hubel, D.H. (1963). Single-cell responses in striate cortex of kittens deprived of vision in one eye. J. Neurophysiol. *26*, 1003–1017.

Williams, K., Russell, S.L., Shen, Y.M., and Molinoff, P.B. (1993). Developmental switch in the expression of NMDA receptors occurs in vivo and in vitro. Neuron *10*, 267–278.

Wray, N.R., Ripke, S., Mattheisen, M., Trzaskowski, M., Byrne, E.M., Abdellaoui, A., Adams, M.J., Agerbo, E., Air, T.M., Andlauer, T.M.F., et al.; eQTLGen; 23andMe; Major Depressive Disorder Working Group of the Psychiatric Genomics Consortium (2018). Genome-wide association analyses identify 44 risk variants and refine the genetic architecture of major depression. Nat. Genet. *50*, 668–681.

Wu, Y.E., Pan, L., Zuo, Y., Li, X., and Hong, W. (2017). Detecting activated cell populations using single-cell RNA-seq. Neuron *96*, 313–329.e6.

Xi, Y., and Li, W. (2009). BSMAP: whole genome bisulfite sequence MAPping program. BMC Bioinformatics *10*, 232.

Xue, M., Atallah, B.V., and Scanziani, M. (2014). Equalizing excitation-inhibition ratios across visual cortical neurons. Nature *511*, 596–600.

Yap, E.L., and Greenberg, M.E. (2018). Activity-regulated transcription: bridging the gap between neural activity and behavior. Neuron *100*, 330–348.

Zang, C., Schones, D.E., Zeng, C., Cui, K., Zhao, K., and Peng, W. (2009). A clustering approach for identification of enriched domains from histone modification ChIP-seq data. Bioinformatics *25*, 1952–1958.

Zhang, Y., Liu, T., Meyer, C.A., Eeckhoute, J., Johnson, D.S., Bernstein, B.E., Nusbaum, C., Myers, R.M., Brown, M., Li, W., and Liu, X.S. (2008). Model-based analysis of ChIP-seq (MACS). Genome Biol. *9*, R137.

Zhu, Q., Liu, N., Orkin, S.H., and Yuan, G.C. (2019). CUT&RUNTools: a flexible pipeline for CUT&RUN processing and footprint analysis. Genome Biol. *20*, 192.

Please cite this article in press as: Stroud et al., An Activity-Mediated Transition in Transcription in Early Postnatal Neurons, Neuron (2020), https://doi.org/10.1016/j.neuron.2020.06.008

STAR★METHODS

KEY RESOURCES TABLE

REAGENT or RESOURCE	SOURCE	IDENTIFIER
Antibodies		
Rabbit anti-MECP2	Chen et al., 2003	N/A
Rabbit anti-H3K27ac	Abcam	Cat# ab4729
Rabbit anti-GFP	Thermo Fisher	Cat# G10362
Rabbit anti-ARID1A	Cell signaling	Cat #12354
Rabbit anti-H3K4me1	Abcam	Cat # ab8895
Rabbit IgG	Cell Signaling	Cat #2729S
Biological Samples		
Unmethylated lambda DNA	Promega	Cat# D1521
Chemicals, Peptides, and Recombinant Proteins		
Kanic acid	Sigma Aldrich	Cat# K0250
Dynabeads Protein G	Thermo Fisher	Cat# 10004D
Dynabeads Protein A	Thermo Fisher	Cat# 10002D
Agencourt AMPure XP beads	Beckman Coulter	Cat# A63881
Formaldehyde	Sigma Aldrich	Cat# F8775
Concanavalin A beads	Bangs Laboratories	Cat# BP531
protein-A-MNase	Skene and Henikoff, 2017	N/A
Critical Commercial Assays		
Ovation Ultralow Library System	Nugen	Cat# 0330, 0331, 0344
TruSeq Strand Specific RNA-Sequencing kit	Illumina	Cat# RS-122-2101
NEBNext Ultra Directional RNA Library Prep Kits	New England Biolabs	Cat# E7420L
NEBNext Multiplex Oligos for Illumina	New England Biolabs	Cat# E7335L
NEBNext rRNA Depletion Kit	New England Biolabs	Cat# E6310X
Qubit dsDNA HS Assay Kit	Thermo Fisher	Cat# Q32854
Nextera DNA sample kit	Illumina	Cat# FC-121-1030
Chromium TM Single Cell 3′ Library kit v2	10X Genomics	PN-120236
Deposited Data		
Raw data for sequencing	NCBI Gene Expression Omnibus	GSE150538
Experimental Models: Organisms/Strains		
Mouse: C57BL/6 WT	The Jackson Laboratory	N/A
Mouse: C57BL/6 WT	Charles River	N/A
Mouse: *Nestin-cre*	The Jackson Laboratory	Cat# 003771
Mouse: *Dnmt3a*$^{fl/fl}$	Kaneda et al., 2004	N/A
Mouse; *Sst-cre*	The Jackson Laboratory	Cat# 013044
Mouse: *Vip-cre*	The Jackson Laboratory	Cat# 010908
Mouse: *Mecp2* KO	The Jackson Laboratory	Cat# 003890
Mouse: SPRET/EiJ	The Jackson Laboratory	Cat#001146
Mouse: SUN1-2xsfGFP-6xMYC	The Jackson Laboratory	Cat# 021039
Oligonucleotides		
10X_Enrich_R1_F: CTACACGACGCTCTTCCG	This study	N/A

(*Continued on next page*)

Please cite this article in press as: Stroud et al., An Activity-Mediated Transition in Transcription in Early Postnatal Neurons, Neuron (2020), https://doi.org/10.1016/j.neuron.2020.06.008

Continued

REAGENT or RESOURCE	SOURCE	IDENTIFIER
10X_Enrich_HS2_R2_R: GTGACTG GAGTTCAGACGTGTGCTCTTCCG ATCTACGAGTCGGATCTCCCTTT	This study	N/A
Recombinant DNA		
Kir2.1-T2A-TdTomato	Xue et al., 2014	Addgene 60598
Kir2.1mut-T2A-TdTomato	Xue et al., 2014	Addgene 60644
pAAV-hSyn-DIO	Krashes et al., 2011	Addgene 44362
Software and Algorithms		
Bowtie V1	Langmead et al., 2009	http://bowtie-bio.sourceforge.net/index.shtml
SICER	Zang et al., 2009	N/A
BSmap V2.74	Xi and Li, 2009	https://code.google.com/archive/p/bsmap/
DAVID V6.8	Huang et al., 2009	https://david.ncifcrf.gov/
Tophat2	Kim et al., 2013	https://ccb.jhu.edu/software/tophat/index.shtml
HTseq	Anders et al., 2015	https://pypi.org/pypi/HTSeq
DEseq	Anders et al., 2015	http://bioconductor.org/packages/release/bioc/html/DESeq.html
Seurat	Satija et al., 2015	https://satijalab.org/seurat/
Monocle	Trapnell et al., 2014	http://cole-trapnell-lab.github.io/monocle-release/
Trimmomatic	Bolger et al., 2014	http://www.usadellab.org/cms/?page=trimmomatic
MACS2	Zhang et al., 2008	https://github.com/macs3-project/MACS/tree/master/MACS2
Irreproducible Discovery Rate (IDR) pipeline from ENCODE	Landt et al., 2012	https://www.encodeproject.org/software/idr/
HOMER	Heinz et al., 2010	http://homer.ucsd.edu/homer/
edgeR	Robinson et al., 2010	https://bioconductor.org/packages/release/bioc/html/edgeR.html
GREAT	McLean et al., 2010	http://great.stanford.edu/public/html/
bbmap	sourceforge.net/projects/bbmap/	https://jgi.doe.gov/data-and-tools/bbtools/
Lapels	Huang et al., 2014	http://csbio.unc.edu/CCstatus/index.py?run=Pseudo

RESOURCE AVAILABILITY

Lead Contact

Further information and requests for resources and reagents should be directed to and will be fulfilled by the Lead Contact, Michael E. Greenberg (michael_greenberg@hms.harvard.edu).

Materials Availability

This study did not generate new unique reagents.

Data and Code Availability

The accession number for the sequencing data reported in this paper is GEO: GSE150538.

EXPERIMENTAL MODEL AND SUBJECT DETAILS

Mice

Animals were handled according to guidelines approved by the Harvard University Standing Committee on Animal Care. Mice were housed in the animal facility with a 12 hour light/dark cycle. Homozygous SUN1-2xsfGFP-6xMYC (Sun1) mice were reported in a

previous study (Mo et al., 2015) and were crossed to homozygous *Vip-cre* or *Sst-cre* (Taniguchi et al., 2011), or *Rorb-cre* (Harris et al., 2014) mice. For conditional cell-type-specific *Dnmt3a* knockout experiments, *Sst-cre* or *Vip-cre* mice were crossed to *Dnmt3a*$^{fl/fl}$ (Kaneda et al., 2004) and Sun1 mice. Littermate controls were used for all comparisons between wild-type *Sst* neurons (*Sst-cre*; *Dnmt3a*$^{+/+}$; Sun1) to *Sst*-specific *Dnmt3a* cKO (*Sst-cre*; *Dnmt3a*$^{fl/fl}$; Sun1) mice, and wild-type *Vip* neurons (*Vip-cre*; *Dnmt3a*$^{+/+}$; Sun1) to *Vip*-specific *Dnmt3a* cKO (*Vip-cre*; *Dnmt3a*$^{fl/fl}$; Sun1) mice. For whole brain-specific DNMT3A KO experiments, *Nestin*-cre mice (Tronche et al., 1999) were crossed to *Dnmt3a*$^{fl/fl}$ mice. *Mecp2* KO mice have been previously described (Guy et al., 2001). Genders were mixed for each experiment. Each nuclear isolation experiment was performed pooling at least two mice. The exception was for the *Dnmt3a* conditional knockout experiments, where one mutant mouse was used for each nuclear isolation, along with gender-matched littermate wild-type controls.

METHOD DETAILS

INTACT nuclear isolation

Cortices were homogenized with a dounce-homogenizer and tight pestle 15 times in 5 mL Buffer HB (0.25M sucrose, 25mM KCl, 5mM MgCl2, 20mM Tricine-KOH pH7.8, 1mM DTT, 0.15 mM spermine, 0.5 mM spermidine, Roche protease inhibitor tablets, 10mM Sodium Butyrate, 1mM Rnase Inhibitor when doing downstream RNA-seq). IGEPAL CA-630 (Sigma) was added to a final concentration of 0.3% to the homogenate, followed by douncing 5 more times with tight pestle. Homogenized cortices were filtered through a 40um strainer then combined with Working Solution (5 volume of OptiPrep + 1 volume of Diluent [150 mM KCl., 30 mM MgCl2, 120 mM Tricine-KOH pH 7.8]) at a 1:1 ratio. The mixture was underlaid with 1.2 mL 30% and 1.2 mL 40% OptiPrep gradient solutions (Working solution and diluted with HB Buffer to 30% or 40%). Following ultracentrifugation, 1 mL of nuclei were collected from the interface of the 30% and 40% Optiprep layers. 1 mL nuclei were pre-cleared with pre-washed 20 μl Protein G Dynabeads (Thermo Scientific) for 30 min rotation at 4°C. Note that the beads were pre-washed twice, each time with 800 μl Wash Buffer (0.25M sucrose, 25mM KCl, 5mM MgCl2, 20mM Tricine-KOH pH7.8, 0.4% IGEPAL CA-630, 1mM DTT, 0.15 mM spermine, 0.5 mM spermidine, Roche protease inhibitor tablets, 10mM Sodium Butyrate, 1mM Rnase Inhibitor when doing downstream RNA-seq). After preclearing, beads/nuclei mixtures were bound to magnet, and the 1 mL nuclei were removed to a new tube. The beads were resuspended with 400 μl wash buffer, then bound to magnet before the resulting supernatant was added to the previous tube containing the nuclei. Each immunoprecipitation (IP) reaction was set up in one tube with the following mixture: ~700 μl nuclei, 400 μl Wash Buffer, 2.5 μl anti-GFP antibody (ThermoFisher Scientific G10362, RRID: AB_2536526). The IP reactions were incubated for 30 minutes rotating at 4°C. After incubation, 60 μl pre-washed beads were added to each IP reaction, followed by an additional 20 minutes rotation at 4°C. Next, the samples, now containing nuclei-bound beads, were placed on magnet for no longer than 1 minute, then put on ice for ~15 s before resuspending the beads by very gentle inversion. The samples were put back on the magnet for no longer than 1 minute, then one ice for ~15 s before gentle resuspension by inversion. This magnet-ice-resuspension pattern was repeated 6-7 times. The samples were then placed on the magnet, and the supernatant was supplanted with 800 μl Wash Buffer, followed by gentle pipetting to resuspend. The samples were put on ice for ~15 s, then after pipetting 1-2 times, the 800 μl sample was added to 8 mL wash buffer. The nuclei-bound beads were washed two more times with additional 10 mL wash buffer first, then 2.5 mL wash buffer. The immunoprecipitated nuclei (bound to beads) were resuspended in 800 μl wash buffer by gentle pipetting. We note that unlike tissue dissociation (Hrvatin et al., 2018), our nuclear isolation approach is not susceptible to ectopic upregulation of activity-induced genes (Fernandez-Albert et al., 2019; Hu et al., 2017; Wu et al., 2017), and therefore did not require additional inhibitors described in Hrvatin et al. (2018).

Nuclear RNA-seq

RNA from INTACT-purified nuclei was extracted with TRIzol (Invitrogen) and purified with a RNeasy kit (on-column DNase treatment) (QIAGEN) following manufacturer's instructions. Libraries were generated with either the Truseq Strand Specific RNA-Sequencing kit (Illumina) or the NEBNext Ultra Directional RNA Library Prep Kits (NEB).

Chromatin immunoprecipitation sequencing (ChIP-seq)

INTACT-purified nuclei were crosslinked in 1% formaldehyde, followed by the addition of 0.125M glycine to stop crosslinking activity. The nuclei were washed with cold 1XPBS, then lysed once with L1 buffer (50mM HEPES pH7.5, 140mM NaCl, 1mM EDTA, 1mM EGTA, 0.25% Triton X-100, 0.5% NP40, 10% Glycerol, protease inhibitors, sodium butyrate), followed by an incubation in L2 buffer (10mM Tris-HCl pH8.0, 200mM NaCl, protease inhibitors, sodium butyrate). The nuclei were resuspended in L3 buffer (10 mM Tris-HCl pH8.0, 100 mM NaCl, 1 mM EDTA, 0.5 mM EGTA, 0.1% Na-Deoxycholate, 0.5% N-lauroylsarcosine, protease inhibitors, sodium butyrate) and sonicated with a Bioruptor (Diagenode) for 40 cycles of 30 s "on" and 45 s "off." Sonicated chromatin were centrifuged at 13,000 rpm for 10 minutes at 4°C to remove insoluble pellet, and then pre-cleared by incubating with Protein A Dynabeads (Thermofisher) for 2 hours at 4°C. Pre-cleared chromatin were incubated with Dynabeads conjugated to H3K27ac (Abcam ab4729, RRID:AB_2118291) or H3K4me1 (Abcam ab8895, RRID:AB_306847) antibodies overnight at 4°C. Beads were washed twice each with Low Salt buffer (0.1% SDS, 1% Triton X-100, 20mM Tris HCl pH8.0, 150mM NaCl, 2mM EDTA), High Salt buffer (0.1% SDS, 1% Triton X-100, 20mM Tris HCl pH8.0, 500mM NaCl, 2mM EDTA) and LiCl buffer (250mM LiCl, 1% NP40, 1mM EDTA, 10mM TrisHCl pH8.0, 1% Sodium Deoxycholate) at 4°C, and washed once with 1XTE buffer at room temperature. Immunoprecipitated

Please cite this article in press as: Stroud et al., An Activity-Mediated Transition in Transcription in Early Postnatal Neurons, Neuron (2020), https://doi.org/10.1016/j.neuron.2020.06.008

chromatin was first eluted off the beads with 1XTE+1%SDS at 65°C with shaking for 30 minutes, and then was de-crosslinked overnight at 65°C. RNaseA was added to each sample, followed by an incubation at room temperature for 30 minutes. The samples were incubated with proteinase K for two to three hours at 55°C with shaking. Immunoprecipitated DNA was purified using phenol-chloroform-isoamyl alcohol followed by QIAGEN MinElute columns. Sequencing libraries were generated by using Ovation Ultralow Library Systems (Nugen) following manufacturer instructions. Libraries were sequenced on an Illumina Nextseq 500.

Assay for Transposase Accessible Chromatin (ATAC)-seq

INTACT-purified nuclei were resuspended in L1 buffer (50mM HEPES pH7.5, 140mM NaCl, 1mM EDTA, 1mM EGTA, 0.25% Triton X-100, 0.5% NP40, 10% Glycerol, protease inhibitors, sodium butyrate), and centrifuged at 2000 rpm at 4°C. L1 buffer was removed, and INTACT-purified nuclei were incubated with Tn5 in TD buffer (Illumina) for 30 minutes at 37°C. Adaptor-ligated DNA fragments were purified using the QIAGEN MinElute kit, and subsequently PCR-amplified with the Nextera DNA sample kit using the following conditions: (1) 5 minutes at 72°C, (2) 1 minute at 98°C, (3) 15 s at 98°C, (4) 30 s at 63°C, (5) one minute at 72°C, (6) Go to step 3 eleven times, (7) hold at 10°C. To control for potential biases for Tn5 toward specific sequence compositions, we performed the above assay on naked genomic DNA isolated from cortices. All ATAC-seq libraries were sequenced on a Nextseq 500.

Whole genome bisulfite-sequencing (WGBS)

WGBS libraries on INTACT-purified nuclei were generated by using a similar method as previously described (Stroud et al., 2017). Briefly, genomic DNA including unmethylated lambda DNA (0.5%; Promega D1521) were sonicated to 200bp using a Covaris S2 or M220, and NEXTflex methylated adapters (Bioo Scientific) were ligated onto the sonicated DNA. The libraries were bisulfite-treated using the EZ DNA methylation-Gold kit (Zymo). The final libraries were sequenced on a Nextseq 500.

In vivo HiChIP on isolated neuronal subtypes

Vip or *Sst*-expressing nuclei were INTACT-isolated and cross-linked using 1% formaldehyde as described above. HiChIP experiments were performed as previously described (Mumbach et al., 2016) with the following modifications to the protocol: (1) 4 μl of MboI was used to digest chromatin. (2) Sonication step was performed using Covaris M220 (Millitube) PIP 75; Duty factor 5%; CPB 200; Time 2 minutes. (3) For the IP step, 2 μl of anti-H3K27ac antibodies (Abcam ab4729, RRID:AB_2118291) and 20 μl of Protein A Dynabeads (Thermofisher) were used. (4) For adding Illumina sequencing adapters to samples, we used 0.05 μl of Tn5 (Illumina) to each sample and amplified for 12 cycles using the Nextera DNA sample kit (Illumina). All libraries were paired-end sequenced on a Nextseq 500.

Kainic acid (KA) treatment

Three-week-old *Vip-cre*; Sun1 mice were injected intraperitoneally with either kainic acid (Sigma Aldrich K0250) (~4mg/kg) or 1X PBS for controls. The cortices were dissected and processed two hours post-injection.

Dark rearing and Light exposure experiments

Mice were dark-housed for two weeks. For light exposure, mice were transferred to the light chamber for three hours prior to dissecting the visual cortex. Dark-reared control mice were not exposed to light and sacrificed in the dark. Eyes from all animals were enucleated prior to dissecting the tissue.

KIR2.1 overexpression experiment

Kir2.1-T2A-TdTomato (RRID:Addgene_60598) or Kir2.1mut-T2A-TdTomato (RRID:Addgene_60644) (Xue et al., 2014) sequences were cloned into a pAAV-hSyn-DIO backbone (Addgene 44362) and packaged into AAV2/9 viruses. AAVs were generated at the Boston Children's Hospital Viral Core. When neurons are infected with the virus, KIR2.1 or KIR2.1mut proteins would only express in the presence of Cre. Therefore, by infecting the AAVs to *Sst*-cre; Sun1 mice the KIR2.1 or KIR2.1mut proteins would be overexpressed only upon infecting *Sst* neurons. Intracerebroventricular (ICV) injections of either Kir2.1 or Kir2.1mut AAVs were performed on postnatal day one *Sst*-cre; Sun1 mice. Infected mice were matured for seven weeks and then perfused with RNAlater (Sigma), and cortices were harvested and incubated in RNAlater overnight at 4°C.

Nuclei isolation followed by CUT&RUN

Cortices from *Sst*-cre; Sun1 or *Vip*-cre; Sun1 mice were collected and homogenized with a dounce-homogenizer and tight pestle 15 times in 5 mL Buffer HB (0.25M sucrose, 25mM KCl, 5mM MgCl2, 20mM Tricine-KOH pH7.8, 1mM DTT, 0.15 mM spermine, 0.5 mM spermidine, Roche protease inhibitor tablets, 10mM Sodium Butyrate, 1mM RNase Inhibitor when doing downstream RNA-seq). IGEPAL CA-630 (Sigma) was added to a final concentration of 0.3% to the homogenate, followed by douncing 5 more times with tight pestle. Homogenized cortices were filtered through a 40um strainer then combined with Working Solution (5 volume of OptiPrep + 1 volume of Diluent [150 mM KCl., 30 mM MgCl2, 120 mM Tricine-KOH pH 7.8]) at a 1:1 ratio. The mixture was underlaid with 1.2 mL 30% and 1.2 mL 40% OptiPrep gradient solutions (Working solution and diluted with HB Buffer to 30% or 40%). Following ultracentrifugation, 1 mL of nuclei were collected from the interface of the 30% and 40% Optiprep layers. Draq 5 (Abcam) was used to stain DNA. Using a Sony SH800Z Cell sorter, GFP positive nuclei (using Sun1-GFP on nuclear membrane) were selected

and sorted into CUT&RUN wash buffer (1 mL of 1M HEPES pH 7.5, 1.5 mL of 5M NaCl, 1 mL of 10% Tween-20, 0.05 g BSA, 25 μl of 1M spermidine, protease inhibitors (Roche), H2O to 50 mL). Nuclei were bound to concanavalin A-coated (ConA) beads that were washed once with CUT&RUN binding buffer (1 mL of 1M HEPES pH 7.9, 500 μl of 1M KCl, 50 μl of 1M CaCl2, 50 μl of 1M MnCl2, H2O to 50 mL). ConA-bead-bound nuclei were incubated overnight in cold CUT&RUN antibody buffer (1 mL CUT&RUN Triton-wash buffer, 4 μl of 0.5M EDTA) with either in-house anti-FOS antibodies (E.L., M.G.Y., M.E.G., and T. Vierbuchen, unpublished data), anti-ARID1A (Cell signaling #12354, RRID:AB_2637010) or IgG (Cell Signaling #2729S, RRID:AB_1031062). After incubation, the ConA-bead-bound nuclei were washed once with CUT&RUN antibody buffer, and protein-A-MNase (Skene and Henikoff, 2017) was added to each sample to a final concentration of 700 ng/mL, followed by an incubation for one hour at 4°C. The ConA-bead-bound nuclei were washed twice with CUT&RUN Triton-wash buffer (1 mL of CUT&RUN wash buffer, 10 μl of 10% Triton X-100), and resuspended in 100 μl Triton wash buffer. To each sample, 3 μl of 0.1M CaCl2 was added to each sample, and incubated on ice for 30 min. The reaction was stopped by adding 100 μl 2x STOP buffer (68 μl of 5M NaCl, 40 μl of 0.5M EDTA, 8 μl of EGTA, 4 μl 10% Triton X-100, 2 μl of 1 pg/ul yeast spike-in DNA, 10 μl of RNase A, H2O 868 μl) and incubating at 37°C for 20 minutes. Two μl of 10% SDS was added to the supernatant and the samples were proteinase K treated for > 2 hours at 65°C. DNA was collected by ethanol precipitation. Library preparation was performed as previously described (Hainer and Fazzio, 2019), except that Rapid Ligase (Enzymatics) was used for adaptor ligation, and AMPure XP beads were used for the cleanup of the final libraries. All CUT&RUN libraries were paired-end sequenced (40 bases x 2) on a Nextseq 500.

Whole cortex CUT&RUN

Cortices from adult Mecp2 KO and littermate wild-type controls, or adult Nestin-cre; *Dnmt3a*$^{fl/fl}$ and littermate wild-type controls (*Dnmt3a*$^{fl/fl}$) were collected and homogenized with a dounce-homogenizer and tight pestle 15 times in 5 mL Buffer HB (0.25M sucrose, 25mM KCl, 5mM MgCl2, 20mM Tricine-KOH pH7.8, 1mM DTT, 0.15 mM spermine, 0.5 mM spermidine, Roche protease inhibitor tablets, 10mM Sodium Butyrate, 1mM RNase Inhibitor when doing downstream RNA-seq). IGEPAL CA-630 (Sigma) was added to a final concentration of 0.3% to the homogenate, followed by douncing 5 more times with tight pestle. Homogenized cortices were filtered through a 40um strainer, and centrifuged at 500 g at 4°C. The nuclei were resuspended in CUT&RUN wash buffer, and CUT&RUN experiments were performed as described above using anti-MECP2 antibodies (Chen et al., 2003), anti-H3K27ac antibodies (Abcam ab4729, RRID:AB_2118291) and IgG (Cell Signaling #2729S, RRID:AB_1031062).

Fluorescence-activated cell sorting (FACS) for single-nuclei RNA-seq

Sst-cre; Sun1 or *Vip*-cre; Sun1 mouse cortices were harvested and fixed in RNAlater overnight at 4°C. Cortices were homogenized with a dounce-homogenizer and tight pestle 15 times in 5 mL Buffer HB (0.25 M sucrose, 25 mM KCl, 5 mM MgCl2, 20 mM Tricine-KOH pH7.8, 1mM DTT, 0.15 mM spermine, 0.5 mM spermidine, Roche protease inhibitor tablets, 10mM Sodium Butyrate, 1 mM Rnase Inhibitor when doing downstream RNA-seq). IGEPAL CA-630 (Sigma) was added to a final concentration of 0.3% to the homogenate, followed by douncing five more times with tight pestle. Homogenized cortices were filtered through a 40 μm strainer, and centrifuged at 500 g to pellet the nuclei. The nuclei were resuspended in FACS buffer (1XPBS, 1% BSA) and sorted on GFP-positive nuclei (using Sun1-GFP localized throughout the nuclear membrane) were sorted into cold FACS buffer using a Sony SH800Z Cell sorter. All single nuclei RNA sequencing experiments were performed using the Chromium TM Single Cell 3′ Library kit v2 (10X Genomics) following manufacturer instructions. For KIR2.1 overexpression experiments, the viral transcripts were PCR amplified. This additional step was necessary because in any given nuclei only a small proportion of the total transcripts are captured in a high-throughput single-cell RNA-seq experiment. Therefore, amplification of viral transcripts enabled better determination of whether a neuron was infected by AAVs or not. After the cDNA amplification step in the manufacturer protocol, we set aside 5% of the total sample, and viral transcripts were amplified with HS_10X_Enrich_R1_F (CTACACGACGCTCTTCCG) and HS_10X_Enrich_HS2_R2_R (GTGACTGGAGTTCAGACGTGTGCTCTTCCGATCTACGAGTCGGATCTCCCTTT) using Q5 High-Fidelity 2X Master Mix (NEB). The PCR products were cleaned up with AMPure XP beads, and were sample-index PCR amplified according to manufacturer instructions (10X Genomics). All libraries were sequenced for 26 cycles and 58 cycles on a Nextseq 500.

Luciferase reporter experiments

Embryonic (E14) CGEs or mixed cortical neurons (E16) were dissected, dissociated and cultured as previously described (Malik et al., 2014). At days *in vitro* (DIV) 5, plasmids were transfected using Lipofectamine 2000 (Life Technologies) following manufacturer instructions. At DIV6, neurons were silenced overnight by the application of one uM TTX and 100uM AP5 to the cultures. At DIV7, the cultures were depolarized by KCl (55mM) for six hours and then harvested. The cell lysates were processed following manufacturer instructions (Promega), and were measured using a BioTek Synergy 4 multi-detection microplate reader. Firefly luciferase readings for each well of cultures were normalized to Renilla luciferase readings. The normalized Firefly readings were averaged across two to three wells (technical replicates).

Please cite this article in press as: Stroud et al., An Activity-Mediated Transition in Transcription in Early Postnatal Neurons, Neuron (2020), https://doi.org/10.1016/j.neuron.2020.06.008

Allele-specific quantification of H3K27ac in C57BL/6J and SPRET/EiJ

SPRET/EiJ mice (Jackson Labs #001146) were bred with C57BL/6J mice that were homozygous for the Sun1-GFP and Sst-cre alleles as detailed above. Cortices from 3-week old F1-hybrid mice were harvested and nuclei were purified with INTACT approach detailed above. ChIP-seq was performed with anti-H3K27ac antibodies (Abcam ab4729) and reads were sequenced paired-end with the NextSeq 500.

Illustrations

Illustrations were created with https://biorender.com

QUANTIFICATION AND STATISTICAL ANALYSIS

Statistical analysis

The statistical analyses for each experiment are noted in the figure legends. No methods were used to determine whether the data met assumptions of the statistical approach. No statistical methods were used to predetermine sample sizes. No sample randomization was performed. No blinding of experiments was performed.

Nuclear RNA-seq analysis

Data were analyzed as previously described (Stroud et al., 2017). Briefly, reads were mapped to annotated genes and the genome using Tophat2 (Kim et al., 2013), and quantified with HTseq (Anders et al., 2015). Only uniquely mapping reads were retained, and duplicated reads were discarded. Gene expression levels were quantified by reads per kilobase of transcript per million mapped reads (RPKM). Differential gene expression analysis was performed using DEseq2 (Love et al., 2014) using two biological replicates for each postnatal time point. Genes that change in expression were defined using > 2fold and FDR < 1e-4 cutoffs. Gene ontology analyses were performed using DAVID (Huang et al., 2009).

ChIP-seq analysis

Reads were trimmed with Trimmomatic (Bolger et al., 2014) using SLIDINGWINDOW:5:30. Reads were then mapped to the mm9 genome with default parameters using Bowtie2 (Langmead et al., 2009) only retaining uniquely mapping reads with samtools (Li et al., 2009) using parameters -h -b -F 3844 -q 10. Two pseudoreplicates comprising 50% of reads were generated with macs2 randsample. Peaks were called from macs2 with pooled reads and with both pseudoreplicate samples (Zhang et al., 2008) using parameters -g mm -p 1e-1–nomodel–extsize 200. High-confidence H3K27ac peaks were identified with the Irreproducible Discovery Rate (IDR) pipeline from ENCODE (Landt et al., 2012) with a threshold FDR < 0.0025. ATAC-seq summits (detailed in following section) were used to center all *cis*-regulatory elements (i.e., enhancers and promoters). HOMER annotatepeaks.pl was used with mm9 -size 1000 -len 200 -noadj to quantify H3K27ac signal ± 500 bp from all ATAC-seq summits genome-wide. DEseq2 (Love et al., 2014) and edgeR (Robinson et al., 2010) were used to define developmentally regulated enhancers by quantifying changes in H3K27ac levels at ATAC-seq peaks across biological replicates between different postnatal time points. For edgeR, the function glmTreat() was used to determine p values. For postnatally regulated H3K27ac regions, we used a 2-fold cutoff and an FDR < 0.01 and we took the intersection of sites that met these criteria in both DEseq2 and edgeR. We lastly defined gene-distal enhancers as those ATAC-seq peaks that overlap H3K27ac regions and are at least one kilobase away from the nearest annotated transcription start sites (ENSEMBL). For gene-ontology analyses of genes closest to distal enhancers, GREAT (McLean et al., 2010) was used using a maximum distance cutoff of 100 kilobases.

ATAC-seq analysis

Reads were trimmed with Trimmomatic (Bolger et al., 2014) using SLIDINGWINDOW:5:30. Reads were then mapped to the mm9 genome with default parameters using Bowtie2 (Langmead et al., 2009) only retaining uniquely mapping reads with samtools (Li et al., 2009) using parameters -h -b -F 3844 -q 10. Two pseudoreplicates comprising 50% of reads were generated with macs2 randsample. Peaks were called from macs2 with pooled reads and with both pseudoreplicate samples (Zhang et al., 2008) using parameters -g mm -p 1e-1–nomodel–extsize 200. High-confidence ATAC-seq peaks were identified with the Irreproducible Discovery Rate (IDR) pipeline from ENCODE (Landt et al., 2012) with a threshold FDR < 0.0025. For motif identification, genomic sequences spanning ± 250 bp of the center of ATAC-seq peaks were analyzed with MEME (Bailey et al., 2009). Of the significantly enriched motifs, motifs that were enriched toward the middle of the ATAC-seq peaks (Bailey and Machanick, 2012) were reported.

Heritability Enrichment Methods

To perform heritability enrichment analysis, we used stratified LD score regression (Finucane et al., 2015); given a functional partition of the genome, the analysis determines whether an annotation carries more genetic heritability than expected based on GWAS summary statistics. We obtained a baseline model of 54 annotations from Finucane et al. and augmented the model with the annotations defined from our analysis of activated, repressed, and constitutive enhancers. Specifically, for each combination of cell line (*Sst* and *Vip*) and trait, we fit two models: 1) activated and constitutive enhancers and 2) repressed and constitutive enhancers. Constitutive enhancers were included in both models to control for the effect of brain-specific enhancers in general. Following the

recommendations of Finucane et al., we excluded the MHC region from analysis and restricted to HapMap3 (Altshuler et al., 2010) SNPs when fitting the model. When comparing enrichment of an annotation across traits, we corrected for multiple hypothesis tests using the Holm step-down procedure. GWAS summary statistics were obtained from the following studies: Schizophrenia (scz) (Schizophrenia Working Group of the Psychiatric Genomics Consortium, 2014), Bipolar (bp) (Bipolar Disorder and Schizophrenia Working Group of the Psychiatric Genomics Consortium, 2018), Major Depressive Disorder (MDD) (Wray et al., 2018) (excludes restricted access samples from 23andMe), Autism spectrum disorder (ASD) (Grove et al., 2019), ADHD (Martin et al., 2018), and RA (Okada et al., 2014). All other summary statistics were obtained from analysis of the UKBiobank (Loh et al., 2018).

WGBS analysis

The reads were mapped to the genome using BSmap (Xi and Li, 2009) retaining uniquely mapping, non-redundant reads. Methylation levels were calculated by taking the ratio between #C and #C+#T basecalls. Postnatal differentially methylated regions (DMRs) across the genome in *Sst* and *Vip* neurons were defined using MOABS software (Sun et al., 2014) (-R -p 8 -g 3 -x 700 -m 100) comparing methylation patterns in P10 and three weeks. The eGREs were defined as increased methylated regions (IMRs) that overlapped with an ATAC-seq peak in one week but lacked an ATAC-seq peak at eight weeks. For whole cortex WGBS analysis, we re-analyzed published whole cortex datasets (Stroud et al., 2017).

HiChIP analysis

Paired-end reads were mapped to the mm9 genome using HiC-Pro (Servant et al., 2015). Duplicated reads were removed and assigned to MboI restriction fragments. Using the HiC-Pro output files, DNA loops were called using Hichipper (Lareau and Aryee, 2018). For each sample, DNA loops called by ten paired-end tags (PET) and FDR < 1e-10 were retained. All loops greater than 1 Mb in length were removed as previously performed (Mumbach et al., 2017). Of these high confidence DNA loops, only those that were identified in two independent biological replicates were retained for analyses.

CUT&RUN analysis

Reads were trimmed with Trimmomatic (Bolger et al., 2014) using SLIDINGWINDOW:5:30. Paired-end trimmed reads were re-paired with the repair.sh utility from bbmap (Bushnell, 2014). Reads were then mapped to the mm9 genome using Bowtie2 (Langmead et al., 2009) with parameters as previously detailed (Skene and Henikoff, 2017) using –local –very-sensitive-local –no-unal –no-mixed –no-discordant –phred33 -I 10 -X 700. Only uniquely mapping reads were retained with samtools (Li et al., 2009) using parameters -h -b -F 3844 -q 10. Two pseudoreplicates comprising 50% of reads were generated with macs2 randsample. Peaks were called from macs2 with pooled reads and with both pseudoreplicate samples (Zhang et al., 2008) using parameters -g mm -p 1e-1–nomodel–extsize 200. High-confidence FOS CUT&RUN peaks were identified with the Irreproducible Discovery Rate (IDR) pipeline from ENCODE (Landt et al., 2012) with a threshold FDR 1e-5. Finally, regions containing perfect AP1 binding motifs (TGASTCA) were considered high confidence FOS-bound sites. To define strong FOS binding sites in Figure S6M, we compared FOS CUT&RUNs to IgG CUT&RUNs using SICER (Zang et al., 2009) with W = 100, G = 100, FDR < 0.001 thresholds for each biological replicate. Of these significantly enriched regions, those with at least a 2-fold enrichment of FOS compared to IgG were ranked based on the FDR, and the top 4000 significantly enriched regions were retained. Next, the intersect between FOS enriched regions between biological replicates were selected, and finally, regions containing perfect AP1 binding motifs (TGASTCA) were selected. For motif analyses, cutruntools (Zhu et al., 2019) was used using default parameters.

Single-nuclei RNA sequencing analyses

Fastq files were generated using mkfastq in Cell Ranger (10X Genomics). Biological replicates were aggregated using the Cell Ranger "aggr" pipeline, and mapped to genes using Cell Ranger "count" pipeline (mm10-1.2.0_premrna). The data were clustered using Seurat (Satija et al., 2015) as previously described (Stroud et al., 2017), except that nuclei with at least 500 genes covered were retained for analyses and genes expressed in at least 3 nuclei were kept for analyses. T-distributed stochastic neighbor embedding (t-SNE) plots and gene expression overlays were generated using the "TSNEplot" and "FeaturePlot" functions, respectively. The transcript counts were normalized such that the sum of all genes in a given nucleus equals 10,000. Differential gene expression in a given cell type was performed using Monocle (Trapnell et al., 2014). For Kir2.1 experiments, nuclei where the viral transcripts represented > 0.2% of total transcripts were determined to be infected by the virus, whereas nuclei where there were no viral transcripts detected were determined to be uninfected by the virus.

Allele-specific mapping of C57BL/6J and SPRET/EiJ reads

The SPRET/EiJ pseudogenome was assembled as detailed in Vierbuchen et al. (2017). Briefly, SNPs in the SPRET/EiJ relative to the mm10 reference genome were annotated with VCFtools, only high-confidence SNPs were retained, and these SNPs were used to construct the SPRET/EiJ pseudogenome with Modtools. Reads were trimmed with Trimmomatic (Bolger et al., 2014) using SLIDINGWINDOW:5:30. Paired-end trimmed reads were re-paired with the repair.sh utility from bbmap (Bushnell, 2014). Each read was mapped in parallel to both the mm10 reference genome or the generated SPRET/EiJ pseudogenome. Reads initially mapped to the SPRET/EiJ pseudogenome were converted back to mm10 reference genome coordinates with Lapels (Huang et al., 2014). BAM files with mapped reads that overlapped at least one SPRET/EiJ SNP were retained for downstream analysis. These reads converted

back into FASTQ files wherein every possible allelic combination of SNPs for each read was represented (up to 2^20 reads). The original reads were only retained if and only if all possible allelic combinations mapped to the same coordinates on the alternate genome. All distal ATAC-seq peaks from C57BL/6J that overlapped H3K27ac peaks (i.e., active enhancers from Figure 2) were examined for consensus AP-1 motifs (TGA[G/C]TCA) (Risse et al., 1989) within the central ± 250 bp. Only those that contained at least one C57BL/6J-specific and zero strain-shared consensus AP-1 motifs were considered for Figure 6E and their coordinates were lifted from mm9 to mm10 with UCSC's liftOver utility. Aggregate plots of H3K27ac read density centered on ATAC-seq summits were generated with HOMER 4.9 and the following parameters: mm10 -size 2000 -hist 10.